

**DESIGN AND SIMULATION OF PULL-IN  
PHENOMENON OF MEMS SWITCHES**

**M.Sc. Thesis by  
Halil TEKİN, B.Sc.  
( 504051106 )**

**Date of submission: 19 April 2007**

**Date of defence examination: 3 May 2007**

**Supervisor (Chairman): Asst. Prof. Dr. Serhat İKİZOĞLU**

**Co-Supervisor: Assoc. Prof. Dr. Levent TRABZON**

**Members of the Examining Committee: Prof.Dr. Ali TOKER**

**Prof.Dr. Serhat ŞEKER**

**Assoc. Prof.Dr. Metin GÖKAŞAN**

**MAY 2007**

**MEMS ANAHTARLARIN KAPANMA OLGUSUNUN  
TASARIM VE SİMÜLASYONU**

**YÜKSEK LİSANS TEZİ  
Müh. Halil TEKİN  
( 504051106 )**

**Tezin Enstitüye Verildiği Tarih : 19 Nisan 2007  
Tezin Savunulduğu Tarih : 3 Mayıs 2007**

**Tez Danışmanları : Yard. Doç.Dr. Serhat İKİZOĞLU  
Doç. Dr. Levent TRABZON**

**Diğer Jüri Üyeleri: Prof.Dr. Ali TOKER  
Prof.Dr. Serhat ŞEKER  
Doç.Dr. Metin GÖKAŞAN**

**MAYIS 2007**

## **ACKNOWLEDGMENT**

I would like to express my deepest appreciation to my supervisors Asst. Prof. Dr. Serhat İKİZOĞLU and Assoc. Prof. Dr. Levent TRABZON for being helpful and sharing their knowledge and experiences during my research.

I want to indicate my sincere gratitude to Tolga KAYA for his valuable and continuous help, and co-operation. Also, I would like to thank Prof. Dr. Ali TOKER for his technical support in the preparation of thesis. I am very grateful to Asst. Prof. Dr. Hür KÖŞER from Yale University because of his kind support and suggestions during this study.

I would like to express my great appreciation to Technological and Research Council of Turkey for the scholarship during my master degree at İstanbul Technical University.

Finally, I would like to dedicate my thesis to my family who paid the greatest sacrifice during my education and especially to my mother who passed away three years ago.

May 2007

Halil TEKİN

## CONTENTS

<b>TABLE LIST</b>	<b>v</b>
<b>FIGURE LIST</b>	<b>vi</b>
<b>ÖZET</b>	<b>ix</b>
<b>SUMMARY</b>	<b>x</b>
<b>1. INTRODUCTION</b>	<b>1</b>
1.1. Background and Motivation	1
1.2. Pull-in Phenomenon in MEMS	2
1.1. Thesis Objectives and Organization	2
<b>2. MEMS OVERVIEW</b>	<b>4</b>
2.1. Introduction	4
2.2. Application of MEMS	4
2.3. MEMS Market and Industry Structure	5
2.4. Analysis and Design Principles of MEMS Devices	7
2.4.1. Principles of MEMS Devices	7
2.4.2. Design Methodology for MEMS	8
<b>3. MODELING AND SIMULATION OF MEMS SWITCHES</b>	<b>10</b>
3.1. The System Concerning MEMS Switch	10
3.2. Pull-in Phenomenon of MEMS Switches	11
3.2.1. Cantilever Beam Equation	13
3.2.2. Pull-in Voltage Closed Form Model	14
3.3. Resonant Frequency Analysis for MEMS Switches	20
3.4. Analysis for Different Sizes	25
3.5. Tip Deflection Analysis	27
3.6. Damping Factor and Response to Accelerations	39
3.7. Hysteresis and Resistance Considerations	45
<b>4. CONCLUSION AND FUTURE WORK</b>	<b>53</b>
<b>REFERENCES</b>	<b>55</b>
<b>APPENDIX A</b>	<b>57</b>
<b>APPENDIX B</b>	<b>60</b>
<b>APPENDIX C</b>	<b>65</b>
<b>APPENDIX D</b>	<b>68</b>
<b>APPENDIX E</b>	<b>69</b>
<b>BIOGRAPHY</b>	<b>70</b>

**TABLE LIST**

	<u>Page No</u>
<b>Table 3.1</b> The Optimum Values of Pull-in Voltage, Width, Length Regarding to Three Different Values of Initial Gap for Fixed Thickness.....	17
<b>Table 3.2</b> The Optimum Values of Pull-in Voltage for Aluminum Cantilever Beam, Width, Length Regarding to Three Different Values of Initial Gap for Fixed Thickness.....	19
<b>Table 3.3</b> The Optimum Values of Pull-in Voltage for Gold Cantilever Beam, Width, Length Regarding to Three Different Values of Initial Gap for Fixed Thickness.....	19
<b>Table 3.4</b> Resonant Frequencies of Polysilicon Cantilever Beam and Fixed-Fixed Beam for Optimum Values of Length (l) and Width (w) and Fixed Values of Thickness (h) and Initial Gap ( $d_0$ ).....	23
<b>Table 3.5</b> Resonant Frequencies of Aluminum Cantilever Beam and Fixed-Fixed Beam for Optimum Values of Length (l) and Width (w) and Fixed Values of Thickness (h) and Initial Gap ( $d_0$ ).....	24
<b>Table 3.6</b> Resonant Frequencies of Gold Cantilever Beam and Fixed-Fixed Beam for Optimum Values of Length (l) and Width (w) and Fixed Values of Thickness (h) and Initial Gap ( $d_0$ ).....	24
<b>Table 3.7</b> The Comparison of Pull-in Point Changes for Conditions Under Vibration and No Vibration .....	39
<b>Table 3.8</b> Common Sources of Vibrations [17].....	39
<b>Table 3.9</b> The Comparison of Critical Damping Constants and Deflections at 10g for Different Cantilever Beams.....	44
<b>Table 3.10</b> Observed Information from Some Papers.....	50
<b>Table 3.11</b> Resistance Values of Cantilever Beams.....	52
<b>Table B.1</b> The Roots of Eq. (B.41).....	63

## FIGURE LIST

	<u>Page No</u>
<b>Figure 2.1</b> : The Content of Micro-Electro-Mechanical Systems [7].....	4
<b>Figure 2.2</b> : Projected Growth of Worldwide MEMS Market [9].....	6
<b>Figure 2.3</b> : 2006 MEMS Market Share Projection [9].....	6
<b>Figure 2.4</b> : Basic Illustration of a MEMS Device [10].....	7
<b>Figure 2.5</b> : Basic Analysis and Design Principles of MEMS [10].....	8
<b>Figure 2.6</b> : Design Trade-Off for MEMS [11].....	8
<b>Figure 3.1</b> : System Overview [13].....	10
<b>Figure 3.2</b> : Harmonic Resonator and Its Frequency Response [14].....	13
<b>Figure 3.3</b> : (a) A Cantilever Beam Separated from a Fixed Ground Plane by a Dielectric Spacer, (b) A Conceptual Diagram Shows the Deformed Beam Due to an Electrostatic Force When Biased Oppositely Using a Constant Drive Voltage [5].....	14
<b>Figure 3.4</b> : Electric Flux Lines of a Cantilever Beam [5].....	14
<b>Figure 3.5</b> : Non-Uniform Profile of the Electrostatic Pressure for a Cantilever beam (left). Uniform Electrostatic Pressure Profile for a Parallel Plate Geometry (right) [5].....	15
<b>Figure 3.6</b> : Linearization of the Electrostatic Force about Zero Displacement [5].....	15
<b>Figure 3.7</b> : The Value Change of Pull-in Voltage for Fixed $h$ and $d_0$ .....	16
<b>Figure 3.8</b> : The Displacement Change Due to the Pull-in Voltage for Case-1.....	17
<b>Figure 3.9</b> : The Displacement Change Due to the Pull-in Voltage for Case-2.....	18
<b>Figure 3.10</b> : The Displacement Change of a Fixed-Fixed Beam Due to the Pull-in Voltage for Case-1.....	18
<b>Figure 3.11</b> : The Displacement Under the Pull-in Voltage for Cantilever Beams Made of Polysilicon, Aluminum and Gold for $l=260\mu\text{m}$ , $w=50\mu\text{m}$ , $h=1\mu\text{m}$ , $d_0=1\mu\text{m}$ .....	20
<b>Figure 3.12</b> : A Cantilever Beam With Mass per Length $\rho$ , Modulus $E$ , and Inertial Moment $I$ .....	20
<b>Figure 3.13</b> : The Value Change of Resonant Frequencies of the Cantilever Beam for Fixed Thickness ( $h$ ) and Initial Gap ( $d_0$ ).....	21
<b>Figure 3.14</b> : For Fixed Thickness ( $h$ ) and Initial Gap ( $d_0$ ), The Value Change of Resonant Frequencies of the Fixed-Fixed Beam.....	22
<b>Figure 3.15</b> : For Fixed Thickness ( $h$ ) and Initial Gap ( $d_0$ ), The Effective Mass Values of the Cantilever Beam Related to the Different Values of Length ( $l$ ) and Width ( $w$ ).....	22
<b>Figure 3.16</b> : For Fixed Thickness ( $h$ ) and Initial Gap ( $d_0$ ), The Effective Mass Values of the Fixed-Fixed Beam Related to the Different Values of Length ( $l$ ) and Width ( $w$ ).....	23

<b>Figure 3.17</b>	: The Pull-in Voltage Changes for Different Width Values When $l=260\mu\text{m}$ , $h=1\ \mu\text{m}$ , $d_0=1\ \mu\text{m}$ .....	25
<b>Figure 3.18</b>	: The Pull-in Voltage Changes for Different Initial Gap Values When $l=260\mu\text{m}$ , $w=50\ \mu\text{m}$ , $h=1\ \mu\text{m}$ .....	26
<b>Figure 3.19</b>	: The Pull-in Voltage Changes for Different Thickness Values When $l=260\mu\text{m}$ , $w=50\ \mu\text{m}$ , $d_0=1\ \mu\text{m}$ .....	26
<b>Figure 3.20</b>	: A Cantilever Beam Being Affected by a Vibration from Its Base [15].....	27
<b>Figure 3.21</b>	: The Tip Deflection of the Beam When the Base Displacement is $100\mu\text{m}$ at $200\ \text{Hz}$ for $l=260\mu\text{m}$ , $w=50\ \mu\text{m}$ , $d_0=1\ \mu\text{m}$ , and $h=1\mu\text{m}$ .....	28
<b>Figure 3.22</b>	: The Tip Deflection Change for Different Amplitudes of Vibration.....	29
<b>Figure 3.23</b>	: Tip Deflection Values of Beams Made up from Three Materials for $l=260\mu\text{m}$ , $w=50\ \mu\text{m}$ , $h=1\ \mu\text{m}$ , $d_0=1\ \mu\text{m}$ , When a Vibration Affects at Base of the Cantilever Beam that has Amplitude of $100\mu\text{m}$ and Frequency of $200\ \text{Hz}$ .....	29
<b>Figure 3.24</b>	: The Cantilever Beam Deflection Under Force at Free End [15]	30
<b>Figure 3.25</b>	: The Displacement for $l= 260\mu\text{m}$ , $w=50\ \mu\text{m}$ , $d_0=1\ \mu\text{m}$ , and $h=1$ $\mu\text{m}$ .....	31
<b>Figure 3.26</b>	: The Tip Deflection of the Beam When the Base Displacement is $100\mu\text{m}$ at $200\ \text{Hz}$ for $l=260\mu\text{m}$ , $w=50\ \mu\text{m}$ , $d_0=1\ \mu\text{m}$ , and $h=1$ $\mu\text{m}$ and Voltage is $0.95\ \text{Volt}$ .....	32
<b>Figure 3.27</b>	: The Tip Deflection Change for Different Amplitudes of Vibration and for $0.95\ \text{Volt}$ .....	33
<b>Figure 3.28</b>	: The Force Caused by the Tip Deflection When Only Vibration Affects the Beam.....	34
<b>Figure 3.29</b>	: The Comparison of the Displacement Without a Vibration and Under Vibration that has a Force $F= 1.412\times 10^{-9}\ \text{N}$ at the Free End of the Beam.....	34
<b>Figure 3.30</b>	: The Tip Deflection of the Beam Made of Aluminum When the Base Displacement is $100\mu\text{m}$ at $200\ \text{Hz}$ for $l=260\mu\text{m}$ , $w=50$ $\mu\text{m}$ , $d_0=1\ \mu\text{m}$ , and $h=1\ \mu\text{m}$ and Voltage is $0.7\ \text{Volt}$ .....	35
<b>Figure 3.31</b>	: The Force Caused by the Tip Deflection When Only Vibration Affects the Beam Made of Aluminum.....	36
<b>Figure 3.32</b>	: The Comparison of the Displacement Without a Vibration and Under Vibration that has a Force $F= 8.013\times 10^{-10}\ \text{N}$ at the Free End of the Beam Made of Aluminum.....	36
<b>Figure 3.33</b>	: The Tip Deflection of the Beam Made of Gold When the Base Displacement is $100\mu\text{m}$ at $200\ \text{Hz}$ for $l=260\mu\text{m}$ , $w=50\ \mu\text{m}$ , $d_0=1$ $\mu\text{m}$ , and $h=1\ \mu\text{m}$ and Voltage is $0.73\ \text{Volt}$ .....	37
<b>Figure 3.34</b>	: The Force Caused by the Tip Deflection When Only Vibration Affects the Beam Made of Gold.....	38
<b>Figure 3.35</b>	: The Comparison of the Displacement Without a Vibration and Under Vibration that has a Force $F= 1.041\times 10^{-9}\ \text{N}$ at the Free End of the Beam Made of Gold.....	38
<b>Figure 3.36</b>	: The Step Responses for Different Values of Acceleration and Damping Constant for a Cantilever Beam Made of Polysilicon	40

<b>Figure 3.37</b>	: The Step Responses for Different Values of Acceleration at Critical Damping Constant for a Cantilever Beam Made of Polysilicon.....	41
<b>Figure 3.38</b>	: The Step Responses for Different Values of Acceleration at Critical Damping Constant for a Cantilever Beam Made of Aluminum.....	42
<b>Figure 3.39</b>	: The Step Responses for Different Values of Acceleration at Critical Damping Constant for a Cantilever Beam Made of Gold.....	43
<b>Figure 3.40</b>	: The Responses of Polysilicon and Aluminum Cantilever Beams Under 50g Acceleration.....	44
<b>Figure 3.41</b>	: The Response of the Beam Made of Polysilicon to 10g Step Acceleration for Different Damping Ratios.....	45
<b>Figure 3.42</b>	: Model of an Electrostatic Actuator [18].....	46
<b>Figure 3.43</b>	: The Equilibrium Graph [18].....	46
<b>Figure 3.44</b>	: The Graph Leded by $F_{el} + F_{sp} = 0$ Deduces Equilibrium Positions and Pull-in Voltage [18].....	47
<b>Figure 3.45</b>	: The Graph of the Pull-out Situation [18].....	48
<b>Figure 3.46</b>	: The Illustration of the Hysteresis Cycle [18].....	49
<b>Figure 3.47</b>	: (a) The System While Switch is Off (b) The System While the Switch is On Position.....	51
<b>Figure 3.48</b>	: The Resistivity Change of Polysilicon Related to Phosphorus Concentration [23].....	51
<b>Figure 3.49</b>	: The Concept for the Most Suitable Cantilever Beam.....	52
<b>Figure E.1</b>	: The Fabrication Process for the Concept of the Cantilever Beam.....	69

## **MEMS ANAHTARLARIN KAPANMA OLGUSUNUN TASARIM VE SİMÜLASYONU**

### **ÖZET**

Son yıllarda mikro elektromekanik sistemler (MEMS) çok fazla uygulama alanına sahip olmuştur. Savunma, sağlık, otomotiv ve uzay ve havacılık uygulamaları örnek olarak verilebilir. Geniş çaptaki uygulama alanları MEMS'in düşük maliyeti, küçük boyutu ve düşük ağırlığı sonucu ortaya çıkmıştır. Ayrıca MEMS sadece mekanik değil elektriksel parçalar da içermektedir. Bir diğer çok kullanışlı teknoloji titreşim kaynaklarını kullanarak enerji üreten güç harmanlayıcı aletlerdir. İyi bilinmektedir ki, düşük enerji tüketimine ve yüksek izolasyona bağlı olarak, MEMS anahtarlar geleneksel anahtarların yerini almıştır. Bu çalışma bir güç harmanlayıcı sistem için bir MEMS anahtarının tasarım ve simülasyonunu içermektedir. Bu anahtar güç harmanlayıcı sistem tarafından üretilen gerilim ile elektrostatik olarak hareket ettirilir. Bu hareket olayı kapanma olgusunu getirir. Güç harmanlayıcı sistem tarafından üretilen gerilim 0,6-1V gibi düşük bir aralığa sahiptir. Dolayısıyla, kapanma gerilimi aralığına uygun olan kullanılacak anahtarın boyutuna ve malzemesine karar vermek için optimizasyon gerekmektedir. Bu optimizasyonda kapanma gerilimi kapalı formdaki modeli kullanılmaktadır. Bu anahtar rezonans frekanslarından uzakta çalışmalıdır. Bu kısıtlamaya bağlı olarak, rezonans frekans analizi yapılmalıdır ve hangi boyutların ve malzemelerin uygun olduğuna karar verilmelidir. Bunun yanında biz bu anahtardan histeritik bir davranış bekleriz, yani kapanma ve açma gerilimleri farkı olmalıdır. Sistem titreşimli bir ortamda olacağı için sadece elektriksel değil, mekanik analizler de anahtarın dayanıklı olup olmadığına karar vermede büyük rol oynamaktadır. Bu mekanik analizler anahtarın titreşim altındaki uç sapması ve ani ivmelere verdiği basamak cevabı içermektedir. Uç sapmasının analizleri gözlemlendikten sonra titreşim altında kapanma geriliminin değişimleri elde edilebilir. Ani ivmelerin analizi anahtarın ivmeler altında dayanıklı olup olmadığını görmek ve kritik sönüm katsayısının değerini elde etmek için gereklidir. Özel olarak incelen farklı simülasyonlar güç harmanlayıcı sistem için en uygun MEMS anahtarın elde etmek için önemli sonuçlar getirmektedir.

## **DESIGN AND SIMULATION OF PULL-IN PHENOMENON OF MEMS SWITCHES**

### **SUMMARY**

In recent years, micro-electro-mechanical systems (MEMS) have had lots of application areas. Defense, medical, communication, automotive, and aerospace applications can be given as examples. Wide range of application areas has occurred as a result of nearly low-cost, small size and light weight of MEMS. Also, MEMS includes not only mechanical but also electrical components. Another the most useful technology is power harvesting devices using vibration sources to generate energy. It is well known that due to low-power consumption and high isolation, MEMS switches have taken the place of conventional switches. This study contains the design and simulation of a MEMS switch for a power harvesting system. This switch is electro-statically actuated by the voltage generated by the harvesting system. This actuation event brings the pull-in phenomenon. The generated voltage by the power harvester system has a low range that is 0.6-1V. Thus, an optimization is required to decide the size of the switch and the material that will be used that are suitable for pull-in voltage range. For this optimization, a closed form model of pull-in voltage is used. The switch should work far away from resonant frequencies. Due to this constraint, a resonant frequency analysis must be investigated and it is required to decide which sizes and materials are convenient. What is more, we want the switch to have a hysteretic behavior meaning that pull-in and pull-out voltages should be different. As the system will be in a vibrating environment, not only electrical but also mechanical analysis plays a big role to decide whether the switch is robust, or not. These mechanical analyses contain tip deflection of the switch under vibrations and step response under instant accelerations. Observing tip deflection analysis, pull-in voltage changes under vibrations can be obtained. Analysis of instant accelerations is useful to see whether the switch is robust under accelerations or not, and to obtain the critical damping constant value. Several simulations examined particularly bring prominent conclusions to obtain the most suitable MEMS switch for the power harvesting system.

## **1. INTRODUCTION**

### **1.1 Background and Motivation**

In recent years, micro-electro-mechanical systems (MEMS) have made a breakthrough and brought many defense, medical, and commercial applications. Their low cost, small size, low-energy consumption, and life-time have made it so usable in novel devices. The applications of MEMS can be seen in lots of areas of the life [1]. In these areas, most probably they replace traditional devices. For example, in medical applications, MEMS have a wide range of usage such as Bio-mems, hearing and seeing aids, DNA sequencing, and bio-sensors. In information technology, MEMS brought new challenges by enabling smart products. On the other hand, simulation tools have not been developed as much as MEMS [2]. MEMS devices are still being fabricated by trial and error. Since, the design process of MEMS contains different layers such as fluidics, thermal effects, electrostatics, and mechanics. Therefore, these domains are taken into consideration to simulate the performance of finished devices.

Another fast growing area is the energy harvesting systems which are so useful for wireless sensor network nodes. Fixed energy alternatives such as batteries and fuel cells are impractical for wireless devices. There are several power generating devices using solar energy, thermal energy, and vibration based energy. All methods have different requirements; solar methods require enough light energy, thermal methods need enough temperature variation, and vibration-based methods need enough vibration sources. It is clear that vibration sources are more common. Thus, designing an energy harvesting device would be so valuable for long term use that is important for wireless applications.

The interest of this thesis lays in the design of a MEMS switch for a power harvesting system. The main component of this system is a MEMS device with a 100 $\mu\text{m}$  wide, 5 $\mu\text{m}$  thick and 3mm long tethers sharing a 2.5mm wide, 2.5mm long, and 500 $\mu\text{m}$  thick proof-mass [3]. When the system vibrates, an alternating voltage is

generated. Thus, a MEMS switch is required for this system. Since the mid eighties mechanical resonators have been widely used as transducers in mechanical micro sensors [1]. Due to their advantages like low-power consumption, high isolation, MEMS switches replace the conventional switches. Electrostatic actuation is the most preferable actuation method in MEMS because of its simplicity and high efficiency [4]. The pull-in phenomenon that will be examined in this thesis occurs under electrostatic actuation. Also, fundamental frequencies of MEMS switches will be observed. As the power harvesting device will be in a vibrating environment, some dynamic analysis such as tip deflection and step acceleration responses will be investigated. What is more, MEMS switches can be produced from different materials, thus all analyses will be examined for each material in this thesis.

## **1.2 Pull-in Phenomenon in MEMS**

In this section, we give a brief introduction to common phenomenon in MEMS, which is found nearly in the majority of MEMS devices. Thus, before designing a MEMS device, it is prominent to understand this phenomenon. When a voltage is applied to parallel plates, electrostatic force occurs and reduces the gap between these two plates. If voltage increases, eventually two plates touch together. This phenomenon is known as ‘pull-in,’ and the critical voltage associated with it is called ‘pull-in voltage’ [2]. Simulating pull-in structure plays an important role in the design of MEMS devices.

Many models have been presented to model the pull-in phenomenon and the static and dynamic behavior of electrically actuated micro beams. A closed form model for pull-in voltage is given in [5]. Here, we use this closed form model of pull-in voltage to optimize the size of required cantilever beam for power harvesting system generating approximately 0.6-1V. Also, effects of different sizes and different materials on the pull-in point are examined.

## **1.3 Thesis Objectives and Organization**

The objectives of this thesis are:

- To model and simulate accurately the pull-in dynamics, optimize the size of the cantilever beam that is suitable for voltage range of power harvester, and

see the pull-in point change for different materials and different design sizes, and propose a novel MEMS switch actuated by a voltage load lower than the traditionally used voltage.

- To express analytically the natural frequencies of the cantilever beam and fixed-fixed beam, see how different sizes and different materials change their value, and observe if they are suitable for working conditions of power harvesting system.
- To observe the reaction of cantilever beam under sinusoidal vibrations that is important to see whether the switch pulls in before the required voltage, or not, and from this observation obtain the tip deflection of the beam for zero voltage and an applied voltage is less than the pull-in voltage.
- To check the responses of step accelerations affecting the base of the beam, decide whether the beam is robust under different accelerations, or not, and obtain the critical damping constant value that cause an overshoot in the step response of the beam.
- To study the hysteresis cycle of MEMS switches beams having a dielectric space on the ground plane and after observing studies and experiments that have been examined in previous papers, propose a hysteresis range for the cantilever beam we are interested in and to obtain resistance values of cantilever beams and decide which one is suitable.

The organization of the thesis is as follows. In Chapter 2, we present a general overview of MEMS, its wide range of applications and its market and industry structure. Also, we give valuable information about analysis and design principles of MEMS devices. In Chapter 3, we present the modeling and simulation studies of MEMS switch that is required for power harvesting system. In this chapter, thesis objectives are investigated particularly and one by one. Finally, a summary of the conclusions, together with possible future work is given in Chapter 4.

## 2. MEMS OVERVIEW

### 2.1 Introduction

Trend of the developing technology needs new challenges and capabilities to provide the requirements of people. One of fast growing technologies is information systems providing new opportunities for every day life. To bring these opportunities, information systems need sensing and acting capabilities. These needs give a great motivation to research new engineering systems by using MEMS [6].

All components in MEMS have dimensions that are measured in microns. MEMS have different fabrication processes and applications [6]. Fabrication process of MEMS provides the use of integrated electromechanical systems by miniaturization of multiple components. MEMS makes possible the realization of a complete system in a chip enables the development of smart products. Using opportunities of fabrication methods, MEMS involves both mechanical and electrical components as it can be seen in Figure 2.1 [7].

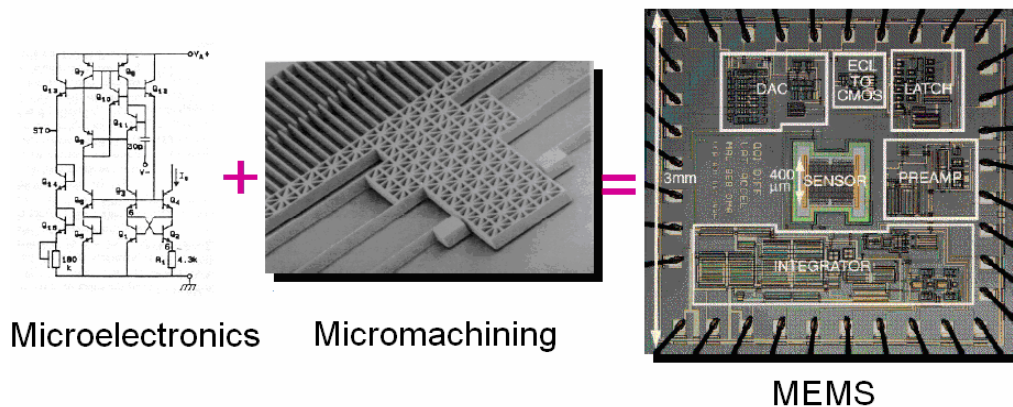


**Figure 2.1:** The Content of Micro-Electro-Mechanical Systems [7]

### 2.2 Application of MEMS

MEMS devices have several applications areas such as automobiles, communication, and medical usage. Because MEMS devices have nearly low-cost, small size and light weight in application systems, they produce new capabilities and increase the

operational performance and lifetimes of existing products and systems. For example, MEMS will make possible complete inertial navigation units on a chip, composed of multiple integrated MEMS accelerometers and gyroscopes [6]. Another example can be given from medical applications as researching new ways and using micro-electromechanical systems to potentially produce complex organs, such as kidneys and livers. In addition to these applications, there are several technologies and products using MEMS [6,8]:

- *distributed unattended sensors* for asset tracking, border control, environmental monitoring, security surveillance and process control,
- *integrated fluidic systems* for miniature analytical instruments, chip-based DNA processing & sequencing, propellant and combustion control, chemical factories on chip,
- *low-power, high-resolution, small-area displays* for workstation and portable, personal information systems,
- *embedded sensors and actuators* for condition-based maintenance of machines & structures and on-demand amplified structural strength in lower-weight systems and disaster-resistant building,
- *mass data storage devices* using magnetic and atomic scale patterning for storage densities of terabytes per square centimeter,
- *integrated micro-opto-mechanical components* for low-power optical communication, displays and fiber-optic switches/modulators, and
- *radio frequency and wireless* for relay & switching matrices, reconfigurable antennas, switched filter banks, electromechanical front-end RF filtering and demodulation

### **2.3 MEMS Market and Industry Structure**

Estimations show that for the near future MEMS products will have a fast increase on all over the world. Recent forecasts imply that the growth of the market potential of MEMS products reaches \$10billion by the year 2006 as it can be seen in Figure 2.2 [9]. This extended growth of MEMS market can be explained as it does not have only one application area. Currently, the majority of MEMS products are

sensors that are used in lots of systems. Thus, advantages of MEMS increase not only its market structure but also market of other sectors using it.

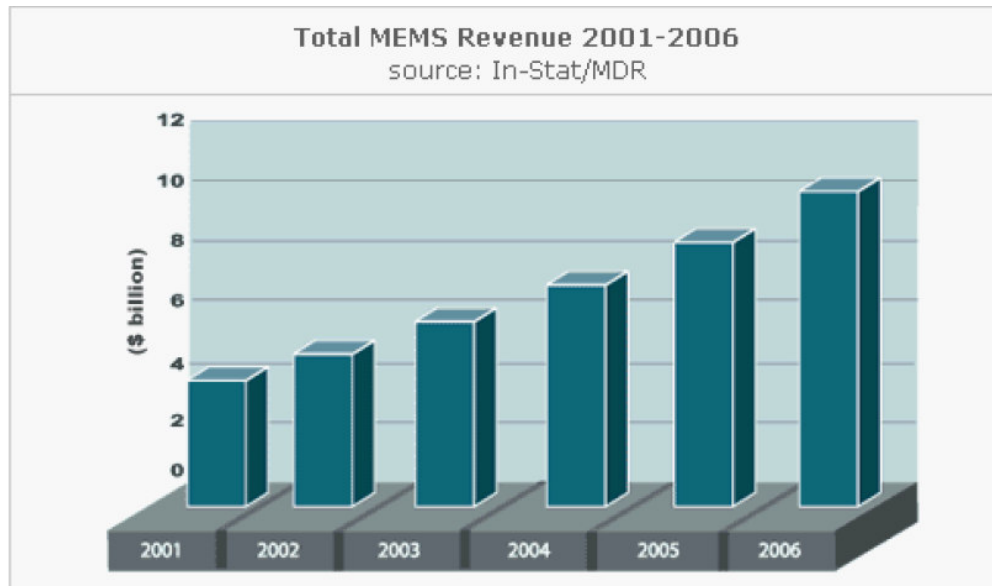


**Figure 2.2:** Projected Growth of Worldwide MEMS Market [9]

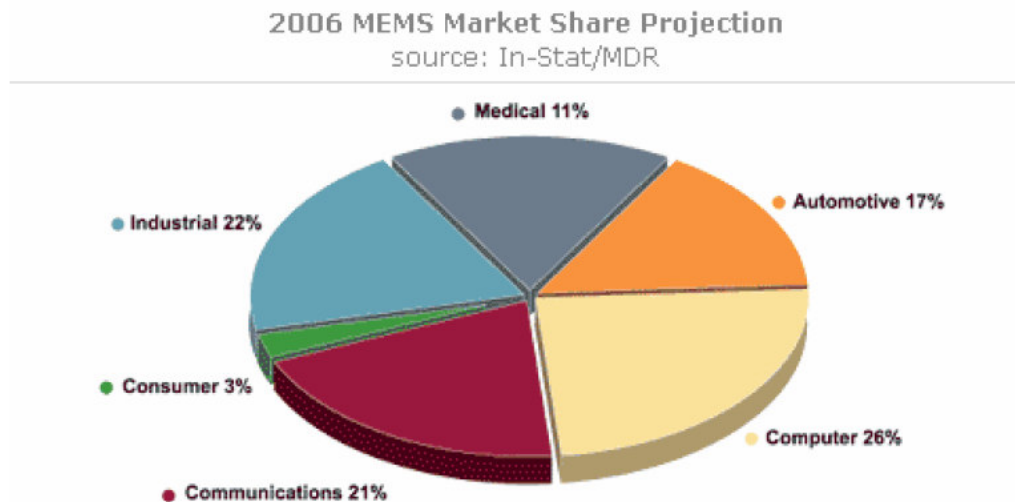


**Figure 2.3:** 2006 MEMS Market Share Projection [9]

The companies producing MEMS products are manufacturers of sensors, industrial and residential control systems, electronic components, automotive and aerospace electronics, and biomedical products. 2006 MEMS market share projection can be seen in the Figure 2.3 [9]. For example, companies fabricating MEMS devices include Honeywell, Motorola, Hewlett-Packard, Analog Devices, Siemens, Hitachi, Texas Instruments, Lucas Xerox, and Rockwell [6]. The current situation of MEMS industry is so strong to provide needs of the world. Also, the

number of MEMS companies is increasing on all over the world. Thus, employment grows in the MEMS industry with demand for new products and solutions using MEMS.

The market and industry structure of MEMS are feeding each other. An increase in one of them causes an increase in other one. May be, in the foreseeable future, MEMS companies will increase and employ lots of people.

## 2.4 Analysis and Design Principles of MEMS Devices

### 2.4.1 Principles of MEMS Devices

Micro-electro-mechanical systems involve micro actuators, micro sensors, and micro electronic circuits as it can be shown in Figure 2.4 [10]. MEMS devices have not only mechanical interaction with surroundings but also electrical or other non-mechanical interaction between their components [10].

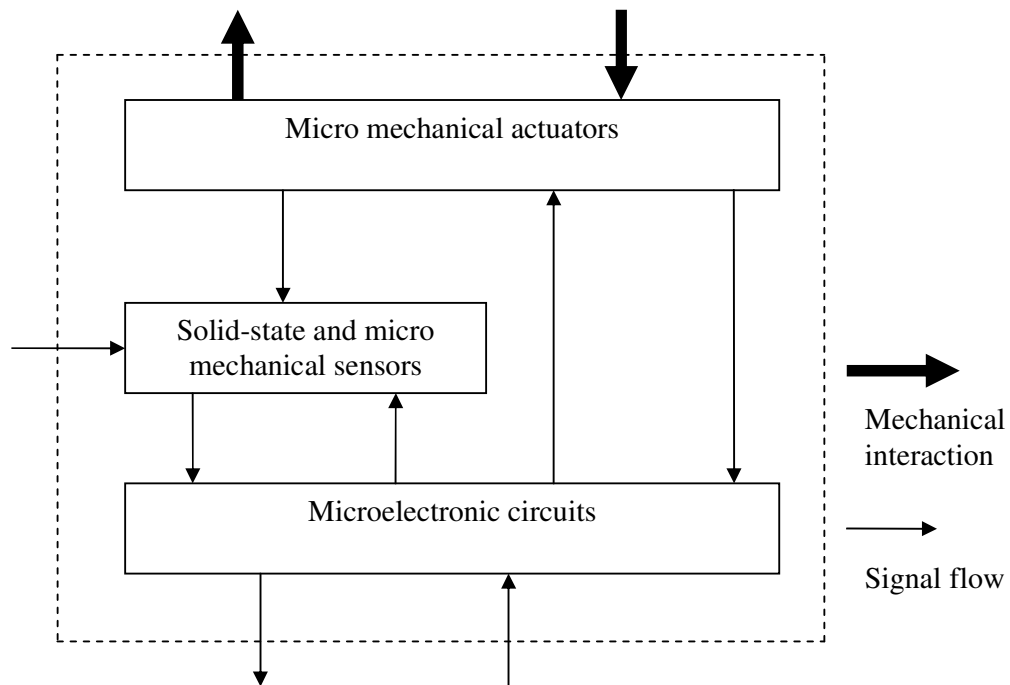


**Figure 2.4:** Basic Illustration of a MEMS Device [10]

In measurement systems, mechanical sensors are used to measure the movement of mechanical structures. Other parameters like temperature, pressure, acceleration can be detected either by mechanical sensors or by solid-

state sensors. Several methods can be used to drive and control micro mechanical actuators. However, recently, the most preferable method is electrostatic actuation. Regarding to given information above, the analysis and design principles of MEMS device can be divided to three basic categories: the dynamics of micro mechanical structure, the sensing scheme and microelectronics, as schematically shown in Figure 2.5 [10]. Needs like 'product performance', 'quality', 'time to produce', 'development cost', 'development risks' have more impact on the development of MEMS products because today's products are more complex [10].

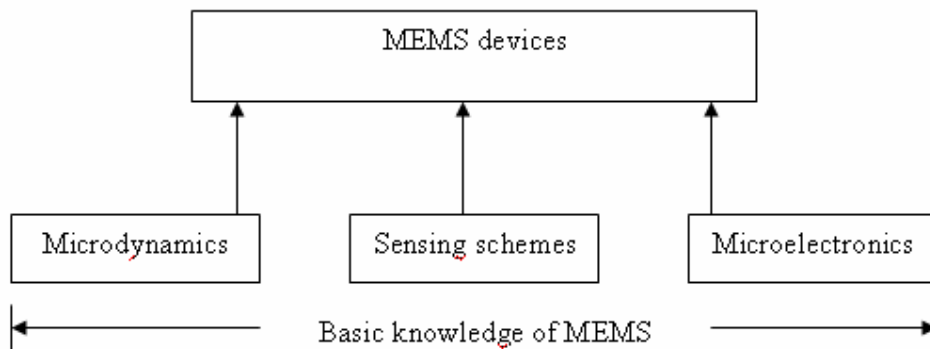


**Figure 2.5:** Basic Analysis and Design Principles of MEMS [10]

**2.4.2 Design Methodology for MEMS**

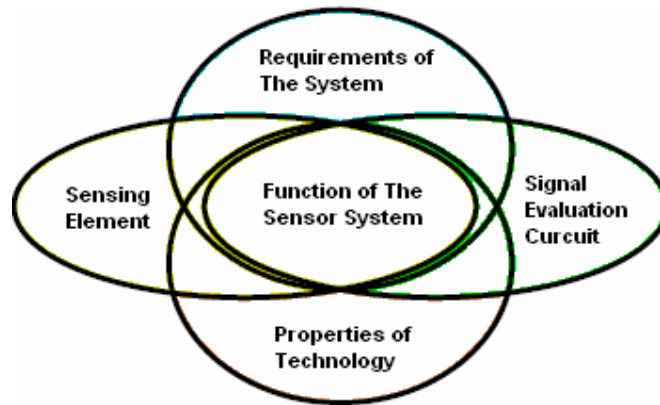


**Figure 2.6:** Design Trade-off for MEMS [11]

There are several effects that should be taken into consideration during the development of MEMS products. These effects are specified by a trade-off as shown in Figure 2.6 [11]. Each part of this relation is related to each other and is

influenced by the others. Design process starts with system requirements by the design on system level [11]. Requirements of the system where MEMS will be used should be analyzed. Then, which sensing element, sensing circuit, and technology provide the needs of the function of the MEMS product should be investigated. Thereby, the manufacturing process can be started. If the components of the product are tested successfully, they are assembled. Thereafter, this process is finished by the fabricated product. Due to some problems during tests, development process does not go forward. The design process of micro electromechanical structures takes time and brings additional costs. Thus, to avoid problems, before fabrication process, simulations should be examined carefully.

### 3. MODELING AND SIMULATION OF MEMS SWITCHES

It is so obvious that several advantages of MEMS switches like low energy consumption, low cost, and easy fabrication have increased their usage instead of traditional switching components and the electrostatic MEM switches applications in micro-electromechanical systems (MEMS). Electrostatic MEM switches play a big role in the function of micro-electromechanical systems [12].

#### 3.1 The System Concerning MEMS Switch

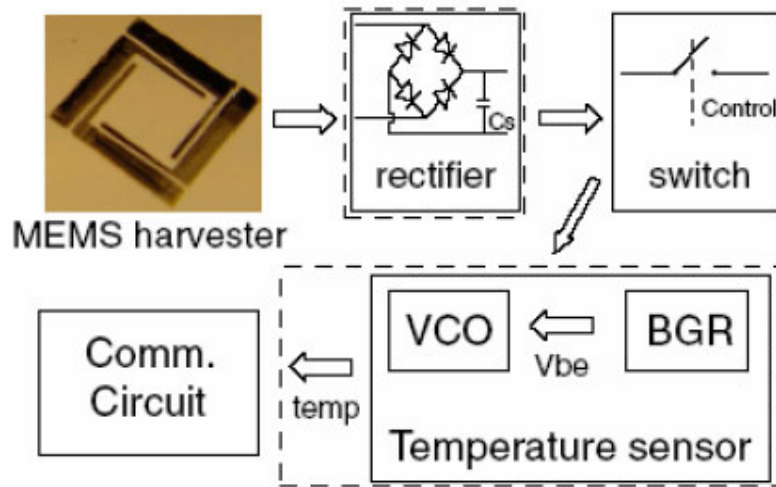


**Figure 3.1:** System Overview [13]

The ultimate goal of this investigation is to design a MEMS switch for a power harvesting system. One of the main components of the harvesting system is a MEMS device with a  $100\mu\text{m}$  wide,  $5\mu\text{m}$  thick and  $3\text{mm}$  long tethers sharing a  $2.5\text{mm}$  wide,  $2.5\text{mm}$  long, and  $500\mu\text{m}$  thick proof-mass. Beams of this device are covered by a thin film of piezoelectric material. So, under vibrations it oscillates and the stress on the piezoelectric material generates an alternating voltage. This voltage is rectified by a diode bridge and stored on a capacitor  $C_s$ . Due to the fact that the voltage on that capacitor changes related to the circuit loading and vibration amplitude, a voltage-controlled switch is required. When the required operational voltage level is

reached, this switch connects the capacitor to the circuitry. When the voltage level is less than this point, the switch is off and the storage capacitor is charged. To prevent damage to the MEMS harvester, the displacement of the cantilever beam is limited by the device's package. The peak-to-peak AC voltage levels of 0.6-1V are possible to be generated by the harvesting system. This voltage range was limited to 1-1.5V in order to make it suitable for use of the sensor circuitry. A bandgap reference circuit is used as a temperature sensor. Temp signal is produced by a voltage controlled oscillator that converts the temperature measurements into a digital square wave. MEMS part of the system has been designed and primary beams were fabricated as shown in Figure 3.1 [13]. Early measurements for the mechanical part indicated that we are able to obtain power levels of  $30\mu\text{W}$  from a  $\text{mm}^3$  device [13]. In this study, the needed MEMS switch is optimized and designed after some observations for pull-in analysis, resonant frequency analysis, effect of the different sizes of the switch, tip deflection analysis, analysis for different materials, damping factor and step responses, and hysteresis and resistance considerations.

### **3.2 Pull-in Phenomenon of MEMS Switches**

Micro cantilever beams are commonly used in MEMS based capacitive-type sensors and actuators. The majority of these devices work in the constant voltage. However, the electrostatic force associated with the applied voltage is nonlinear and brings the well-known phenomenon of 'pull-in' [5]. One of the most important parts of electrostatic MEM actuators is the pull-in phenomenon. Pull-in phenomenon is an instability which is produced by the interaction of the elastic and electrostatic forces when the electrostatic forces are related to the applied voltage. Thus, the applied voltage that causes to pull-in phenomenon can be called "pull-in voltage". In the MEMS switches, the pull-in voltage causes them to close. As a result of the small size of the MEM actuators, other factor such as residual stress in thin films, fringing-field effect and axial stress can affect the pull-in voltage [12]. The determination of the pull-in voltage is important in the sensor or actuator design process to determine the sensitivity, frequency response, and the dynamic response of the switch. Material properties like Young's modulus and the residual stress of micro-fabricated thin films can be decided by using the pull-in voltage [5].

Considering a piston like motion of the beam having a linear spring constant, the widely used parallel-plate approximation method of pull-in voltage calculation says that the pull-in occurs when the movable structure exceeds one-third of the air-gap. This method ignores the effects of the fringing field capacitance. However, for small electrode widths, the fringing field capacitance can cause an increase in the total capacitance [5]. The pull-in voltage of electro-statically actuated cantilever beams can be calculated by using a closed-form model that takes fringing field capacitance into consideration.

MEM switches bring some problems such as high applied voltage, relatively low speed and low power levels. Recently, several studies have been done to solve these problems. To decrease the actuation voltage, some methods can be used such as [12]:

- I. Decreasing the air gap between the fixed plate and the beam
- II. Increasing the electrostatic area
- III. Decreasing the spring constant of the beams

Applying the compressive and tensile axial forces in the fixed-fixed and cantilever beam can be one of the ways to decrease the spring constant of the beams.

Before going the analysis of MEMS switches, it is useful to review the familiar harmonic resonator shown in Figure 3.2 [14].

The equation of motion for a mass-spring-dash pot is

$$m \frac{\partial^2 x}{\partial t^2} + b \frac{\partial x}{\partial t} + kx = F_\omega \cos(\omega t) \quad (3.1)$$

where  $x$  is the motion of the mass  $m$ ,  $b$  damping coefficient,  $k$  is the spring constant, and  $F_\omega$  is the magnitude of the forcing term at frequency  $\omega$  [14]. It is useful to define

resonant frequency  $\omega_0 = \sqrt{\frac{k}{m}}$  and the quality factor  $Q = \frac{\omega_0 m}{b}$ . Solving the Eq. (3.1)

for the amplitude of vibrations gives Eq. (3.2) [14].

$$|X| = \frac{\frac{F_\omega}{m}}{\sqrt{(\omega^2 - \omega_0^2)^2 + \left(\frac{\omega \omega_0}{Q}\right)^2}} \quad (3.2)$$

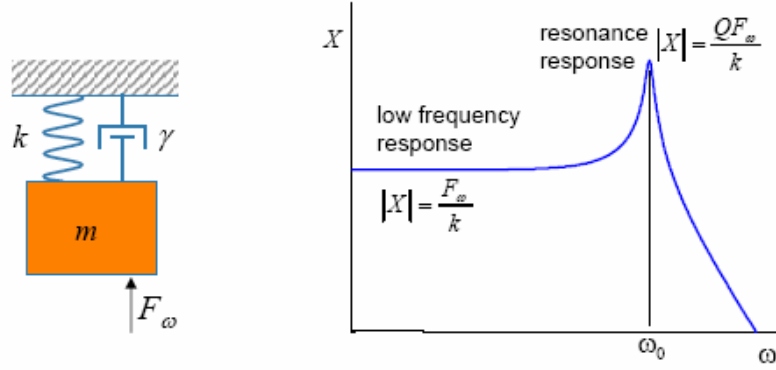


**Figure 3.2:** Harmonic Resonator and Its Frequency Response [14]

### 3.2.1 Cantilever Beam Equation

A typical geometry of a MEMS switch composed of a cantilever beam separated by a dielectric spacer from a fixed ground plane can be seen in Figure 3.3a [5]. As a result of applied voltage, an electrostatic force occurs and causes the beam pull down to the fixed ground plane.

The fixed end of the beam is thought to be at infinity whereas the free end is finite. Under this assumption, the fringing fields at the fixed end can be neglected. Thus, the total capacitance between the cantilever beam and the ground plane consists of the parallel plate capacitance, the fringing field capacitance due to the width of the beam, the fringing field capacitance due to the beam thickness, and the fringing field capacitance at the free end as shown in Figure 3.4 [5].

The capacitance between the cantilever beam and the fixed ground plane can be expressed as:

$$C_{CB} = \epsilon_0 \epsilon_r l \left[ \frac{w}{d_0} + 0.77 + 1.06 \left( \frac{w}{d_0} \right)^{0.25} + 1.06 \left( \frac{h}{d_0} \right)^{0.5} \right] \quad (3.3)$$

where  $l, w$ , and  $h$  represent the length, width, and thickness, respectively [5].  $\epsilon_r$  and  $d_0$  are the dielectric constant and the thickness of the dielectric medium, respectively. After taking fringing field capacitance into consideration, using  $\epsilon_r = 1$  for air, Eq. (3.3) can be modified for the cantilever beam geometry shown in Figure 3.4 as:

$$C_{CB} = \epsilon_0 l \left[ \frac{w}{d_0} + 0.77 + 1.06 \left( \frac{w}{d_0} \right)^{0.25} + 1.06 \left( \frac{h}{d_0} \right)^{0.5} \right] + 1.06 \epsilon_0 w \left( \frac{1}{d_0} \right)^{0.25} \quad (3.4)$$

where the last term in Eq. (3.4) represents the fringing field capacitance at the free end of the beam [5]. The associated electrostatic force where  $V$  is the bias voltage thus can be evaluated from Eq. (3.4) [5].

$$F = -\frac{d}{dz} \left( \frac{1}{2} C_{CB} V^2 \right) \quad (3.5)$$

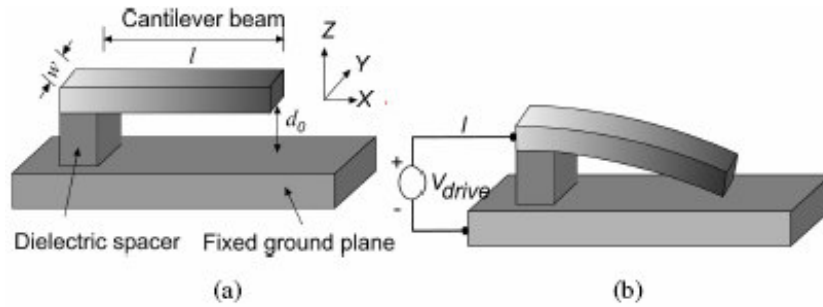


**Figure 3.3:** (a) A Cantilever Beam Separated from a Fixed Ground Plane by a Dielectric Spacer, (b) A Conceptual Diagram Shows the Deformed Beam Due to an Electrostatic Force When Biased Oppositely Using a Constant Drive Voltage [5]

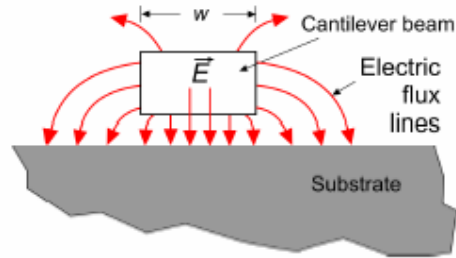


**Figure 3.4:** Electric Flux Lines of a Cantilever Beam [5]

### 3.2.2 Pull-in Voltage Closed Form Model

An expression for a uniform pressure  $P$  causing a cantilever tip deflection of  $z$  can be derived as:

$$P = \frac{Kz}{wl} = \frac{2\tilde{E}h^3}{3l^4} z \quad (3.6)$$

where  $K$  is the spring constant of the beam,  $z$  is the cantilever tip deflection. The effective modulus,  $\tilde{E}$  equals to the plate modulus  $E/(1-\nu^2)$  for wide beams ( $w > 5h$ ) where  $\nu$  represents the Poisson ratio [5]. For narrow beams ( $w < 5h$ ),  $E$  simply becomes the Young's modulus  $E$ . For a cantilever beam, the electrostatic pressure becomes non-uniform due to a redistribution of the charges as the beam

deforms. As a result, the tip of the cantilever will get a higher pressure compared to the region close to the fixed end as shown in Figure 3.5 [5].

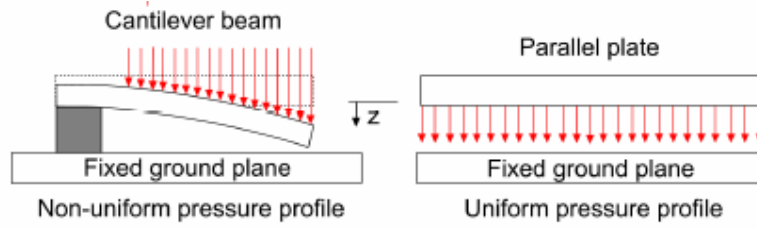


**Figure 3.5:** Non-Uniform Profile of the Electrostatic Pressure for a Cantilever Beam (left). Uniform Electrostatic Pressure Profile for a Parallel Plate Geometry (right) [5]

Thus to calculate the deflection of a cantilever beam actuated by the electrostatic force, it is necessary to obtain a uniform, linear model of the electrostatic force that can be used in Eq. (3.6). A uniform linearized model of the electrostatic pressure can be derived by linearizing the electrostatic force about the zero deflection point, i.e.,  $z_0 = 0$  as shown in Figure 3.6 [5].

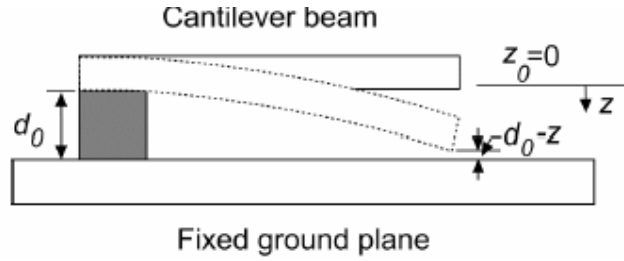


**Figure 3.6:** Linearization of the Electrostatic Force about Zero Displacement [5]

After some linearizations and due to the equilibrium at pull-in, we can obtain the closed-form expression of pull-in voltage  $V_{PI}$  as in [5].

$$V_{PI} = \sqrt{\frac{2\tilde{E}h^3d_0}{8.37\epsilon_0l^4\left(\frac{5}{6(d_0)^2} + \frac{0.19}{(d_0)^{1.25}w^{0.75}} + \frac{0.19}{(d_0)^{1.25}l^{0.75}} + \frac{0.4h^{0.5}}{(d_0)^{1.5}w}\right)}} \quad (3.7)$$

COMSOL Multiphysics program calculates the pull-in voltage by using the following formula,

$$V_{PI} = \sqrt{\frac{4c_1B}{\epsilon_0l^4c_2^2\left(1 + c_3\frac{d_0}{w}\right)}} \quad (3.8)$$

where  $c_1 = 0.07$ ,  $c_2 = 1.00$ , and  $c_3 = 0.42$ ;  $d_0$  is the initial gap between the beam and the ground plane.  $B$  comes from

$$B = \tilde{E}h^3 d_0^3 \quad (3.9)$$

Due to the design constraints, the maximum voltage that can be produced by MEMS harvester is 1 volt. Thus, the pull-in voltage can not take a value more than 1 volt. Our first design constraint is the pull-in voltage. After observing the size values of cantilever beam taken in [5], we have taken the value range of length ( $l$ ) and width ( $w$ ) are  $20\mu\text{m} \leq w \leq 50\mu\text{m}$ ,  $200\mu\text{m} \leq l \leq 500\mu\text{m}$ . For fixed thickness ( $h$ ) and initial gap ( $d_0$ ), the value change of pull-in voltage related to the different values of length ( $l$ ) and width ( $w$ ) can be seen in the Figure 3.7.

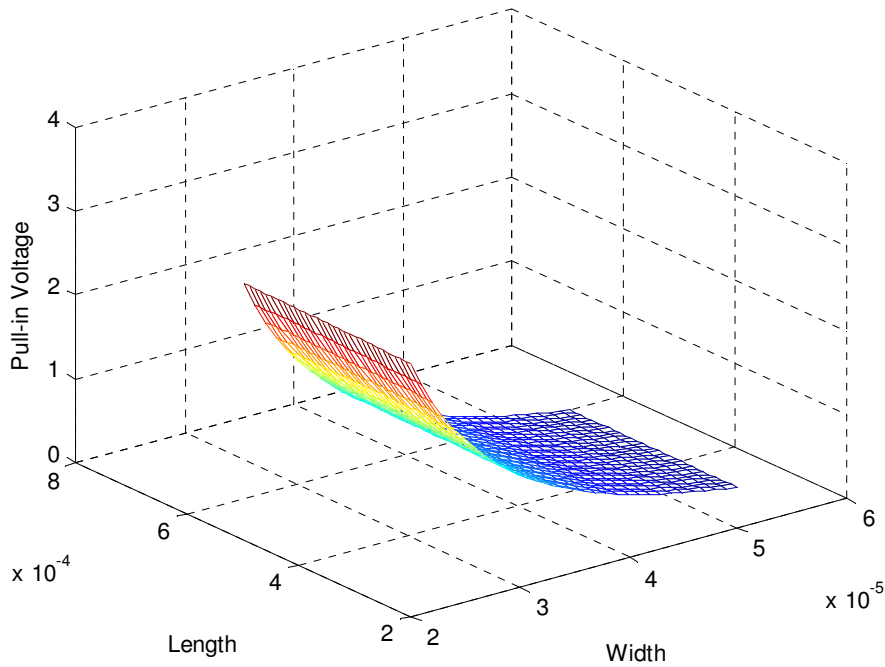


**Figure 3.7:** The Value Change of Pull-in Voltage for Fixed  $h$  and  $d_0$

By using this figure, we can obtain the optimum values of pull-in voltage, width ( $w$ ), and length ( $l$ ). As it is mentioned before, our optimization constraint is that pull-in voltage can not take a value more than 1V. Polysilicon can be used to fabricate the cantilever beam. Its density is  $d = 2330\text{ kg/m}^3$ , Young's modulus  $E = 131 \times 10^9\text{ Pa}$ , Poisson's ratio  $\nu = 0.27$ . Three cases have been checked for fixed thickness ( $h$ ) value and different values of initial gap ( $d_0$ ). Thus, Table 3.1 has been attained related to

the optimization for three cases. MATLAB™ code related to pull-in voltage and its optimization can be seen in Appendix A.

**Table 3.1:** The Optimum Values of Pull-in Voltage, Width, Length Regarding to Three Different Values of Initial Gap for Fixed Thickness

Common Parameters are $E = 131\text{Gpa}$ , $\nu = 0.27$ , $d = 2330\text{ kg/m}^3$ and $h = 1\mu\text{m}$				
	Optimum $V_{PI}$ related to closed form formula	Optimum $V_{PI}$ related to COMSOL Program	Optimum width (w)	Optimum length (l)
Case-1 $d_0 = 1\mu\text{m}$	0.9881 volt	0.9849 volt	50 $\mu\text{m}$	260 $\mu\text{m}$
Case-2 $d_0 = 1.5\mu\text{m}$	0.9978 volt	0.9964 volt	50 $\mu\text{m}$	350 $\mu\text{m}$
Case-3 $d_0 = 2\mu\text{m}$	1 volt	1 volt	24 $\mu\text{m}$	430 $\mu\text{m}$

For case-1 and case-2 and their optimum values, we can simulate the cantilever beam by using Comsol Multiphysics program. Related to the simulation, obtained pull-in graphs are observed as in the Figure 3.8 and Figure 3.9. After obtaining these two figures, it can be said that it is unnecessary to simulate pull-in of the cantilever beam for case-3 where pull-in voltage is equal to 1V.

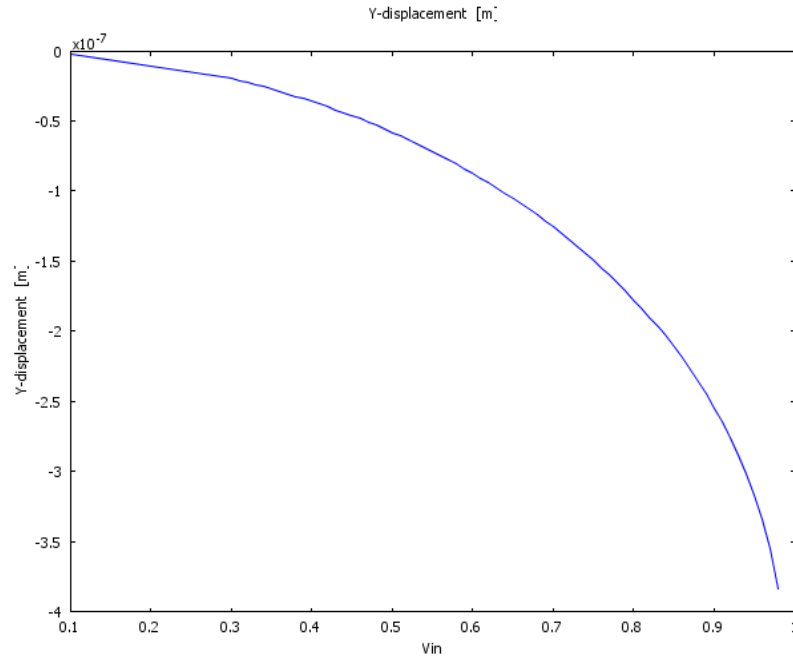


**Figure 3.8:** The Displacement Change Due to the Pull-in Voltage for Case-1

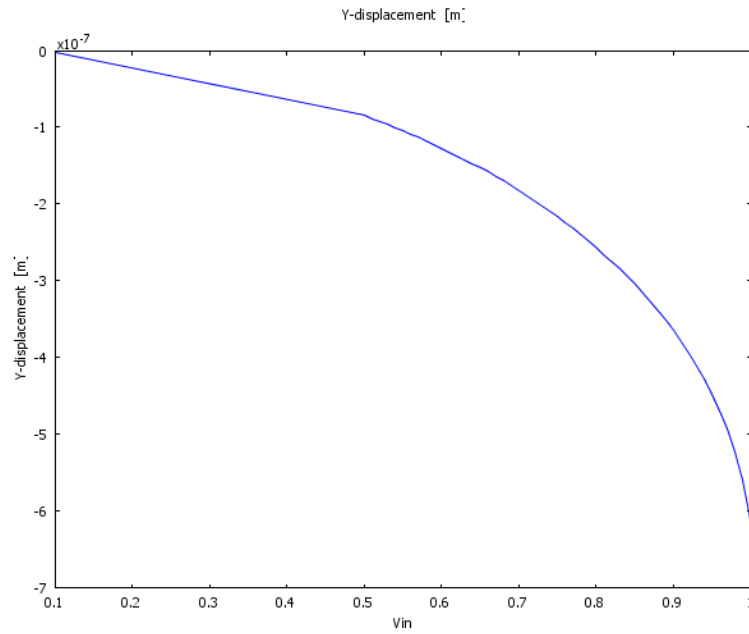


**Figure 3.9:** The Displacement Change Due to the Pull-in Voltage for Case-2

If we make the cantilever beam from Polysilicon, case-1 seems well suited to our design considerations. We know that the required switch for our system can be a fixed-fixed beam. But After observing the pull-in graph for a fixed-fixed beam as in Figure 3.10, it can be said that pull-in point is too high for the voltage range of the power harvesting system.

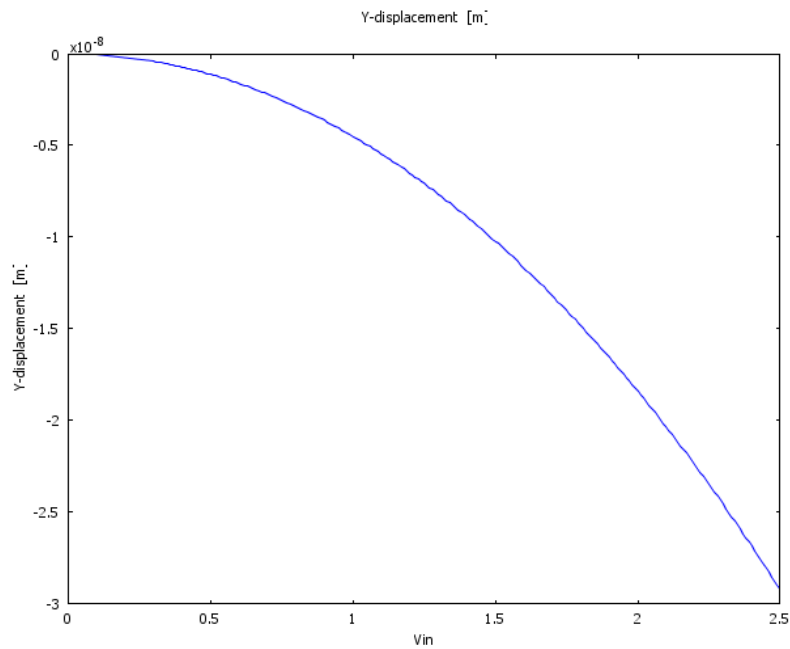


**Figure 3.10:** The Displacement Change of a Fixed-Fixed Beam Due to the Pull-in Voltage for Case-1

We can use different materials for the beam like Aluminum and Gold. The results of optimum values for these materials have been obtained as in the Table 3.2 and Table 3.3. Observing the results in tables, optimum design values for cantilever beams made of Aluminum and Gold are in case-2 where pull-in voltage is less than 1V and pull-in voltages in other cases.

**Table 3.2:** The Optimum Values of Pull-in Voltage for Aluminum Cantilever Beam, Width, Length Regarding to Three Different Values of Initial Gap for Fixed Thickness

Common Parameters are $E = 70 \text{ Gpa}$ , $\nu = 0.33$ , $d = 2700 \text{ kg/m}^3$ and $h = 1 \mu\text{m}$				
	Optimum $V_{PI}$ related to closed form formula	Optimum $V_{PI}$ related to COMSOL Program	Optimum width (w)	Optimum length (l)
Case-1 $d_0 = 1 \mu\text{m}$	1.01 Volt	1.01 Volt	20 $\mu\text{m}$	220 $\mu\text{m}$
Case-2 $d_0 = 1.5 \mu\text{m}$	0.9998 Volt	1.003 Volt	23 $\mu\text{m}$	300 $\mu\text{m}$
Case-3 $d_0 = 2 \mu\text{m}$	1.002 Volt	1.009 Volt	20 $\mu\text{m}$	370 $\mu\text{m}$

**Table 3.3:** The Optimum Values of Pull-in Voltage for Gold Cantilever Beam, Width, Length Regarding to Three Different Values of Initial Gap for Fixed Thickness

Common Parameters are $E = 70 \text{ Gpa}$ , $\nu = 0.44$ , $d = 19300 \text{ kg/m}^3$ and $h = 1 \mu\text{m}$				
	Optimum $V_{PI}$ related to closed form formula	Optimum $V_{PI}$ related to COMSOL Program	Optimum width (w)	Optimum length (l)
Case-1 $d_0 = 1 \mu\text{m}$	0.9897 Volt	0.9865 Volt	50 $\mu\text{m}$	230 $\mu\text{m}$
Case-2 $d_0 = 1.5 \mu\text{m}$	0.997 Volt	0.9955 Volt	50 $\mu\text{m}$	310 $\mu\text{m}$
Case-3 $d_0 = 2 \mu\text{m}$	1 Volt	1 Volt	21 $\mu\text{m}$	380 $\mu\text{m}$

The displacement under the pull-in voltage for cantilever beams made of Polysilicon, Aluminum and Gold for  $l=260\mu\text{m}$ ,  $w=50 \mu\text{m}$ ,  $h=1 \mu\text{m}$ ,  $d_0=1 \mu\text{m}$  can be observed as in the Figure 3.11. Thus, under the same design values making the beam from aluminum brings great advantage regarding to the pull-in voltage. However, to be able to say that we should make the beam from aluminum, other analyses should also be examined.

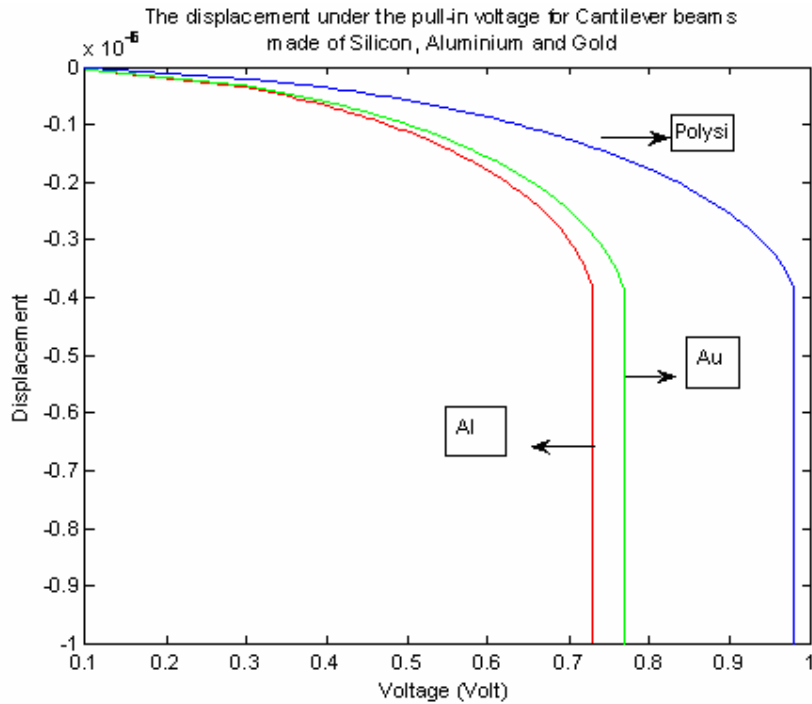


**Figure 3.11:** The Displacement Under the Pull-in Voltage for Cantilever Beams Made of Polysilicon, Aluminum and Gold for  $l=260\mu\text{m}$ ,  $w=50\mu\text{m}$ ,  $h=1\mu\text{m}$ ,  $d_0=1\mu\text{m}$

### 3.3 Resonant Frequency Analysis for MEMS Switches

Resonance is a tendency of a system to oscillate at maximum amplitude at a certain frequency. This frequency is known as the system's natural frequency of vibration, resonant frequency, or eigenfrequency. Regarding to the design considerations, we will examine resonant frequencies of cantilever beams and fixed-fixed beams. Consider a cantilever beam with mass per length  $\rho$  as in Figure 3.12. Assume that the beam has a uniform cross section. The natural frequency formula and the effective mass formula for a cantilever beam is given in Eq. (3.10) and Eq. (3.11), respectively. Obtaining procedure of these two formulas can be observed in Appendix B.

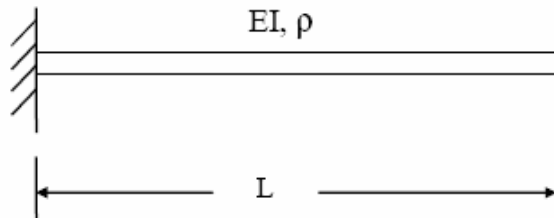


**Figure 3.12:** A Cantilever Beam with Mass per Length  $\rho$ , Modulus  $E$ , and Inertial Moment  $I$

$$f_1 = \frac{1}{2\pi} \left[ \frac{3.5156}{L^2} \right] \sqrt{\frac{EI}{\rho}} \quad (3.10)$$

$$m_{eff} = 0.2427 \rho L \quad (3.11)$$

Consider a fixed-fixed beam with a uniform mass density and a uniform cross section. The natural frequency formula and effective mass formula for a fixed-fixed beam is given in Eq. (3.12) and Eq. (3.13), respectively. Obtaining procedure of these two formulas can be observed in Appendix C.

$$f_1 = \frac{1}{2\pi} \left[ \frac{22.373}{L^2} \right] \sqrt{\frac{EI}{\rho}} \quad (3.12)$$

$$m_{eff} = 0.0959 \rho L \quad (3.13)$$

We can apply the resonant frequency analysis by using these formulas. As it is mentioned before the value ranges of length (l) and width (w) are  $20 \times 10^{-6} \leq w \leq 50 \times 10^{-6}$  and  $200 \times 10^{-6} \leq l \leq 500 \times 10^{-6}$ . For fixed thickness (h) and initial gap ( $d_0$ ), the value change of resonant frequencies of cantilever beam and fixed-fixed beam related to the different values of length (l) and width (w) can be seen in Figure 3.13 and Figure 3.14, respectively. MATLAB<sup>TM</sup> code related to resonant frequency analysis can be seen in Appendix A.

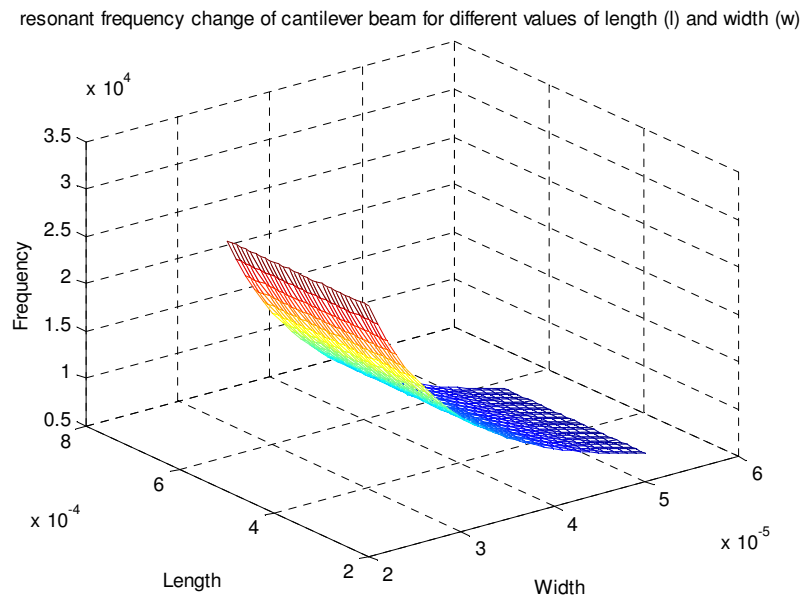


**Figure 3.13:** The Value Change of Resonant Frequencies of the Cantilever Beam for Fixed Thickness (h) and Initial Gap ( $d_0$ )

resonant frequency change of fixed-fixed beam for different values of length (l) and width (w)

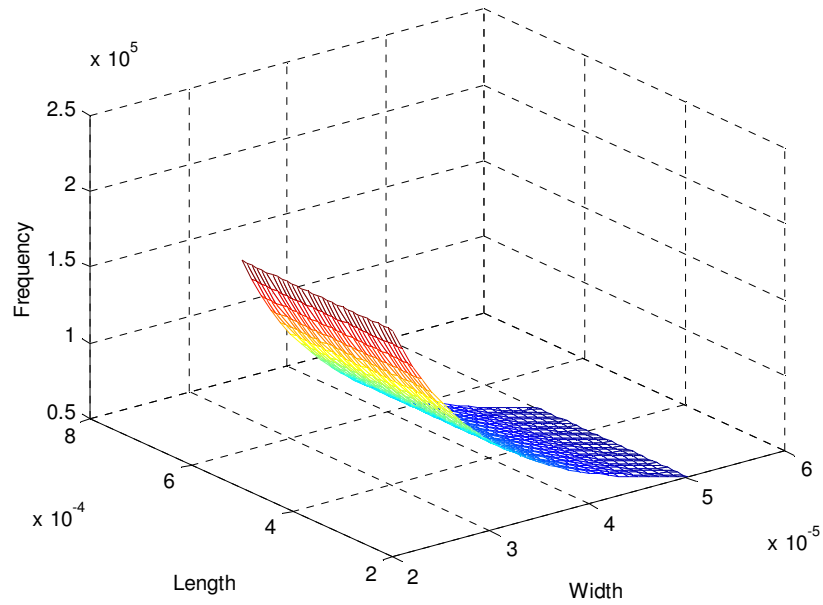


**Figure 3.14:** For Fixed Thickness (h) and Initial Gap ( $d_0$ ), The Value Change of Resonant Frequencies of the Fixed-Fixed Beam

During actuation, not all parts of it move, thus there exists an effective mass for a beam. For fixed thickness (h) and initial gap ( $d_0$ ), the effective mass values of cantilever beam and fixed-fixed beam related to the different values of length (l) and width (w) can be seen in Figure 3.15 and Figure 3.16, respectively.

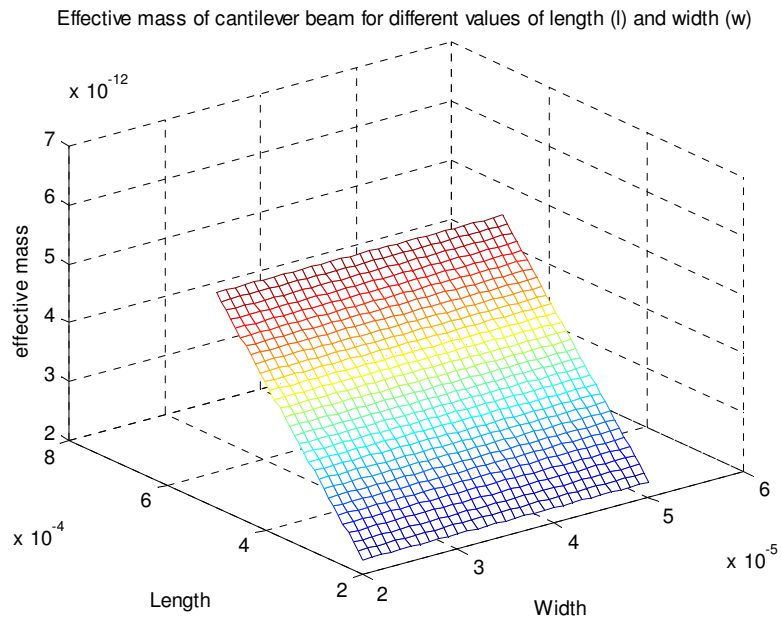


**Figure 3.15:** For Fixed Thickness (h) and Initial Gap ( $d_0$ ), the Effective Mass Values of the Cantilever Beam Related to the Different Values of Length (l) and Width (w)

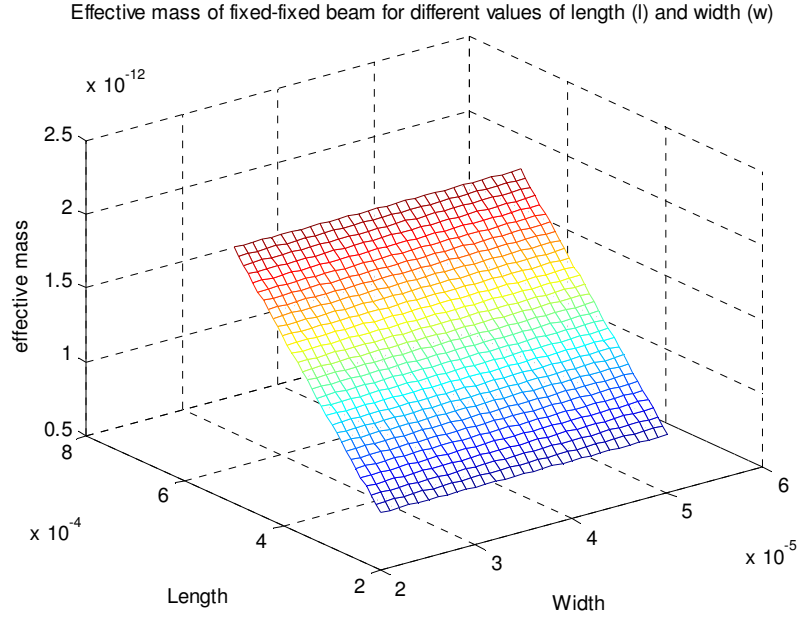


**Figure 3.16:** For Fixed Thickness (h) and Initial Gap ( $d_0$ ), the Effective Mass Values of the Fixed-Fixed Beam Related to the Different Values of Length (l) and Width (w)

After comparing the resonant frequency values obtained from formulas with the results of Comsol, it is seen that all results are same. At this condition we can obtain resonant frequencies of cantilever beam and fixed-fixed beam for optimum values of length (l) and width (w) and fixed values of fixed thickness (h) and initial gap ( $d_0$ ) as in Table 3.4.

**Table 3.4:** Resonant Frequencies of Polysilicon Cantilever Beam and Fixed-Fixed Beam for Optimum Values of Length (l) and Width (w) and Fixed Values of Thickness (h) and Initial Gap ( $d_0$ )

Common Parameters are $E = 131\text{Gpa}$ , $\nu = 0.27$ , $d = 2330\text{ kg/m}^3$ and $h = 1\mu\text{m}$				
	Resonant Frequency of Cantilever Beam	Resonant Frequency of Fixed-Fixed Beam	For Optimum width (w)	For Optimum length (l)
Case-1 $d_0 = 1\mu\text{m}$	18,607 KHz	118,41 KHz	50 $\mu\text{m}$	260 $\mu\text{m}$
Case-2 $d_0 = 1.5\mu\text{m}$	10,268 KHz	65,34 KHz	50 $\mu\text{m}$	350 $\mu\text{m}$
Case-3 $d_0 = 2\mu\text{m}$	6,02 KHz	43,29 KHz	24 $\mu\text{m}$	430 $\mu\text{m}$

**Table 3.5:** Resonant Frequencies of Aluminum Cantilever Beam and Fixed-Fixed Beam for Optimum Values of Length (l) and Width (w) and Fixed Values of Thickness (h) and Initial Gap (d<sub>0</sub>)

Common Parameters are E = 70, ν = 0.33, d = 2700 kg/m <sup>3</sup> and h = 1 μm				
	Resonant Frequency of Cantilever Beam	Resonant Frequency of Fixed-Fixed Beam	For Optimum width (w)	For Optimum length (l)
Case-1 d <sub>0</sub> = 1 μm	12,2 KHz	114,55 KHz	20 μm	220 μm
Case-2 d <sub>0</sub> = 1.5 μm	9,68 KHz	61,60 KHz	23 μm	300 μm
Case-3 d <sub>0</sub> = 2 μm	6.36 KHz	40,49 KHz	20 μm	370 μm

We can use different materials for the beam like Aluminum and Gold. The results of resonant frequency values for these materials have been obtained as in the Table 3.5 and Table 3.6. As it can be seen from the tables, resonant frequencies of cantilever beam and fixed-fixed beam are in the KHz values which are so convenient for operating conditions of the beams. It is prominent that beams should not make significant displacement at these frequencies. These results demonstrate that producing cantilever beam from Polysilicon is the most preferable. However, there is not much difference between resonant frequencies of Aluminum cantilever beam and Polysilicon cantilever beam.

**Table 3.6:** Resonant Frequencies of Gold Cantilever Beam and Fixed-Fixed Beam for Optimum Values of Length (l) and Width (w) and Fixed Values of Thickness (h) and Initial Gap (d<sub>0</sub>)

Common Parameters are E = 70 Gpa, ν = 0.33, d = 19300 kg/m <sup>3</sup> and h = 1 μm				
	Resonant Frequency of Cantilever Beam	Resonant Frequency of Fixed-Fixed Beam	For Optimum width (w)	For Optimum length (l)
Case-1 d <sub>0</sub> = 1 μm	4,55 KHz	41,2 KHz	50 μm	230 μm
Case-2 d <sub>0</sub> = 1.5 μm	3,56 KHz	22,68 KHz	50 μm	310 μm
Case-3 d <sub>0</sub> = 2 μm	2,37 KHz	15,09 KHz	21 μm	380 μm

### 3.4 Analysis for Different Sizes

Analysis for different sizes brings benefits for designing the beam in optimum limits. In this part of the study, we will only work with the cantilever beam made of Polysilicon. Since, it is not important which material is used, the only information we want to know is how different sizes of the cantilever beam make influence on the pull-in voltage. First of all, we will observe the displacement change under the voltage for different width values when  $l=260\mu\text{m}$ ,  $h=1\mu\text{m}$ ,  $d_0=1\mu\text{m}$ . However, at this condition we can see in the Figure 3.17 that the pull-in voltage does not change significantly for width values that are  $20\mu\text{m}$ ,  $50\mu\text{m}$ ,  $100\mu\text{m}$ . Thus, it can be said that increase or decrease in the width value can not change pull-in voltage while other size values are constant.

In the Figure 3.18, we can see how the pull-in voltage changes for different initial gap values when  $l=260\mu\text{m}$ ,  $w=50\mu\text{m}$ ,  $h=1\mu\text{m}$ . It is clear that the required pull-in voltage increases with the increment of the initial gap for  $l=260\mu\text{m}$ ,  $w=50\mu\text{m}$ ,  $h=1\mu\text{m}$ . Thus, the optimum initial gap value for the beam is  $d_0=1\mu\text{m}$  where the pull-in voltage is approximately 1V.

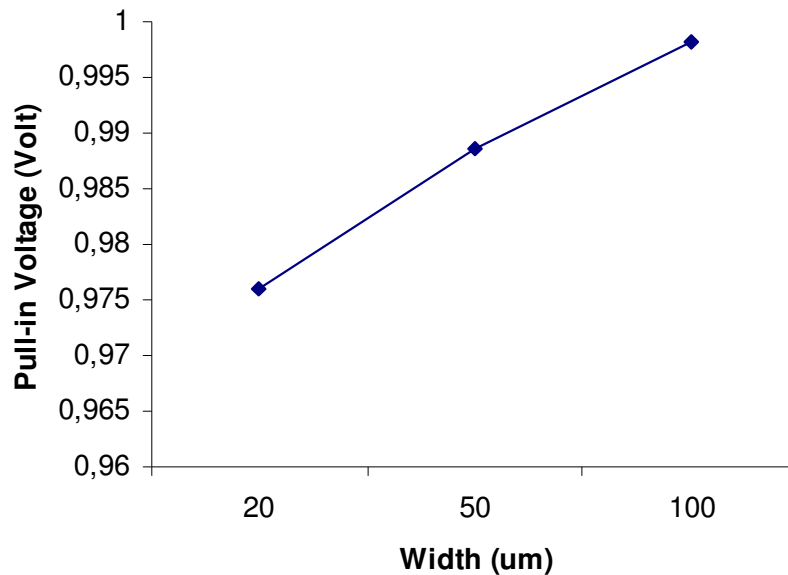


**Figure 3.17:** The Pull-in Voltage Changes for Different Width Values When  $l=260\mu\text{m}$ ,  $h=1\mu\text{m}$ ,  $d_0=1\mu\text{m}$

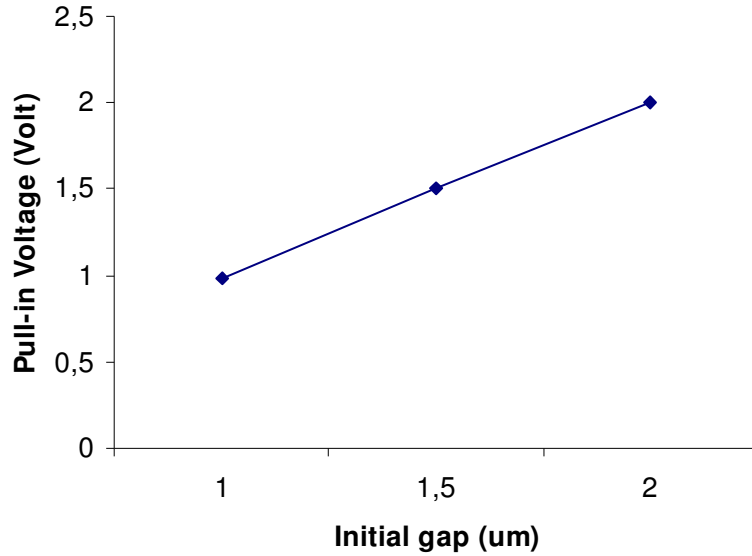


**Figure 3.18:** The Pull-in Voltage Changes for Different Initial Gap Values When  $l=260\mu\text{m}$ ,  $w=50\mu\text{m}$ ,  $h=1\mu\text{m}$

In the Figure 3.19, we can see how the pull-in voltage changes for different thickness values when  $l=260\mu\text{m}$ ,  $w=50\mu\text{m}$ ,  $d_0=1\mu\text{m}$ . It demonstrates that the required pull-in voltage increases with the increment of the thickness for  $l=260\mu\text{m}$ ,  $w=50\mu\text{m}$ ,  $d_0=1\mu\text{m}$ . Thus, the optimum thickness value for the beam is  $h=1\mu\text{m}$  where the pull-in voltage is approximately 1V.

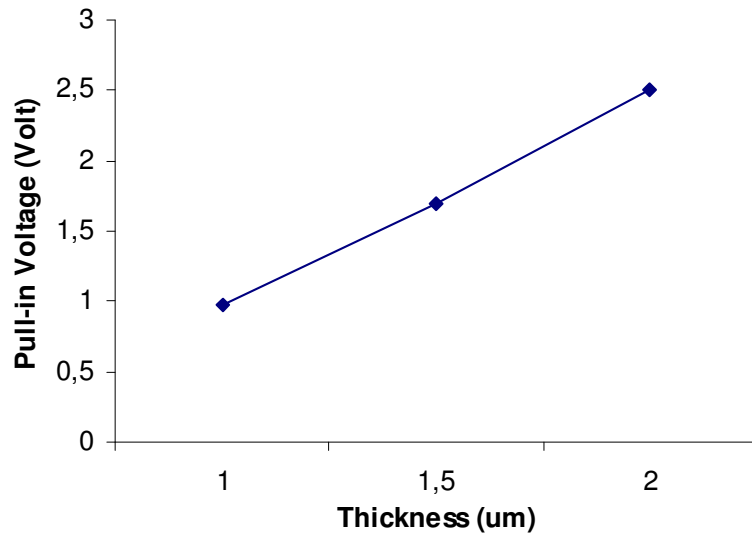


**Figure 3.19:** The Pull-in Voltage Changes for Different Thickness Values When  $l=260\mu\text{m}$ ,  $w=50\mu\text{m}$ ,  $d_0=1\mu\text{m}$

### 3.5 Tip Deflection Analysis

The reaction of cantilever beam should be observed under sinusoidal displacements and step accelerations to the base. From this observation we will obtain tip deflection of the beam that is the difference between the displacements at the free end of the beam and at the fixed end of the beam. Tip deflection is important while designing a MEMS switch. By investigating these parameters, we will be able to make our beam robust. This investigation contains vibration analysis at zero voltage and at voltages less than the pull-in voltage. Applying the superposition method to the tip deflection analysis can be useful that means: firstly, we will assume that voltage is zero and there is a vibration affecting the base of the cantilever beam, then we will assume that there is no vibration and the voltage is less than the pull-in voltage. After calculating tip deflections for both cases, we will add them to obtain the total tip deflection.

At first, we will calculate the tip deflection by assuming voltage is zero and there is a vibration  $V(t)=A_0\sin(\omega t)$  affecting the base of the cantilever beam as in the Figure 3.20 [15].

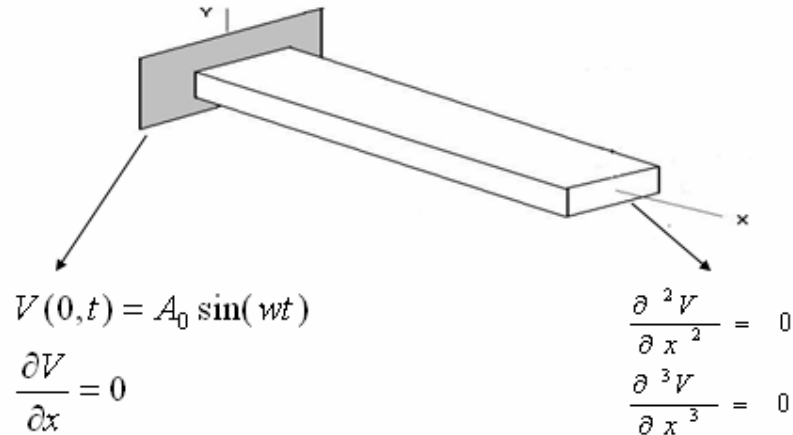


**Figure 3.20:** A Cantilever Beam Being Affected by a Vibration from Its Base [15]

Assuming the Young's modulus  $E$ , the moment of inertia  $I$ , and the cross sectional area  $A$ , the dynamic behavior of cantilever beam can be described as:

$$\rho A \frac{\partial^2 V(x,t)}{\partial t^2} + \alpha \frac{\partial V(x,t)}{\partial t} + \beta I \frac{\partial^5 V(x,t)}{\partial x^4 \partial t} + EI \frac{\partial^4 V(x,t)}{\partial x^4} = 0 \quad (3.14)$$

where  $\rho$  is the mass density of the beam,  $\alpha$  is the mass damping coefficient and  $\beta$  is the stiffness damping coefficient [16]. After obtaining homogenous solution of Eq. (3.14), the tip deflection formula can be expressed as in Eq. (3.15) [16].

$$V(L) = A_0 \frac{\cos kL + \cosh kL}{\cos kL \cosh kL + 1} \quad (3.15)$$

where

$$k^4 = \frac{\omega^2 \rho A - j\omega\alpha}{\beta j\omega + EI} \quad (3.16)$$

In the Figure 3.21, we can observe tip deflection of the beam when the base displacement is  $100 \mu\text{m}$  at  $200 \text{ Hz}$  for case-1 where  $l=260\mu\text{m}$ ,  $w=50 \mu\text{m}$ ,  $d_0=1 \mu\text{m}$ , and  $h=1 \mu\text{m}$ . Also, we can see the tip deflection changes for different amplitudes in the Figure 3.22. MATLAB<sup>TM</sup> code of tip deflection analysis is given in Appendix D.

According to the Figure 3.21, we can say that when a vibration affects the base of the cantilever beam that has amplitude of  $100\mu\text{m}$  and frequency of  $200 \text{ Hz}$ , the tip deflection is  $14.11 \text{ nm}$ . This result is convenient for our design when voltage equals to zero. The tip deflection should also be examined for  $V < V_{\text{pull-in}}$ .

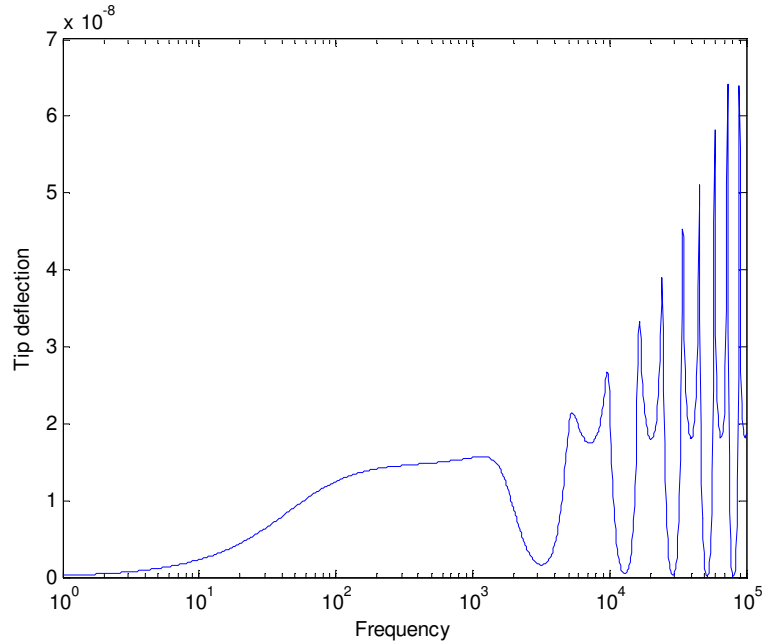


**Figure 3.21:** The Tip Deflection of the Beam When the Base Displacement is  $100\mu\text{m}$  at  $200 \text{ Hz}$  for  $l=260\mu\text{m}$ ,  $w=50 \mu\text{m}$ ,  $d_0=1 \mu\text{m}$ , and  $h=1 \mu\text{m}$

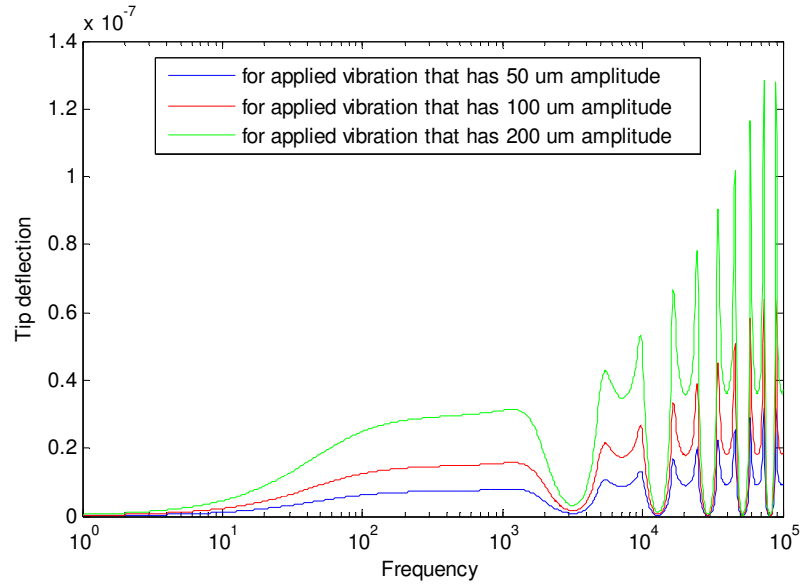


**Figure 3.22:** The Tip Deflection Change for Different Amplitudes of Vibration

It is useful to observe tip deflection values for cantilever beam made of Aluminum and Gold, too. We can see the results in the Figure 3.23. As it can be seen in the figure, the cantilever beam made up from gold has the biggest tip deflections at the resonant frequencies which are greater than 1 KHz.

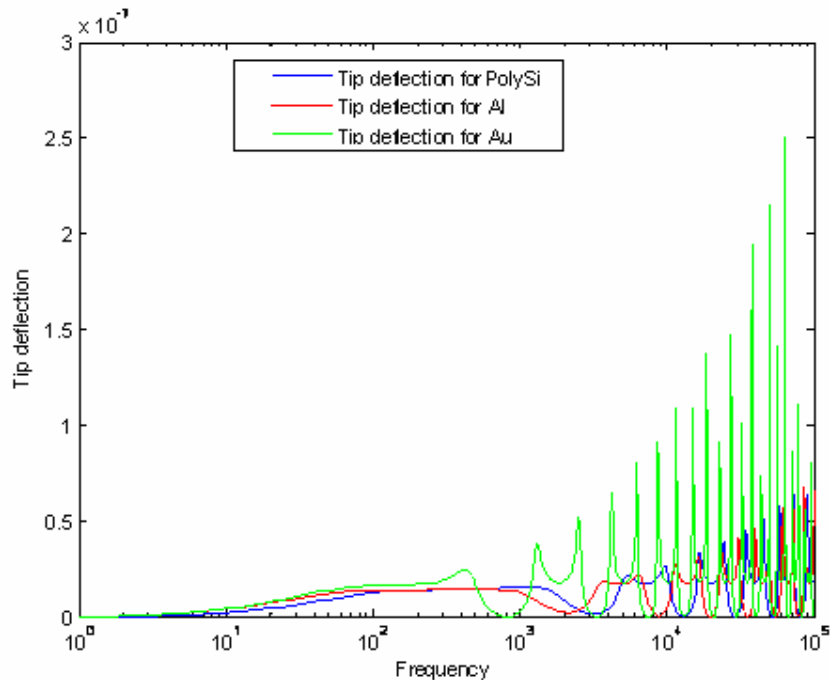


**Figure 3.23:** Tip Deflection Values of Beams Made up from Three Materials for  $l=260\mu\text{m}$ ,  $w=50\mu\text{m}$ ,  $h=1\mu\text{m}$ ,  $d_0=1\mu\text{m}$ , When a Vibration Affects at Base of the Cantilever Beam that has Amplitude of  $100\mu\text{m}$  and Frequency of 200 Hz

In the second case, assuming that there is no vibration and the voltage is not zero, there exists a force  $F$  due to the voltage at the free end of the beam as can be seen in Figure 3.24 [15]. The larger the voltage, the greater the deflection  $v(x)$ .

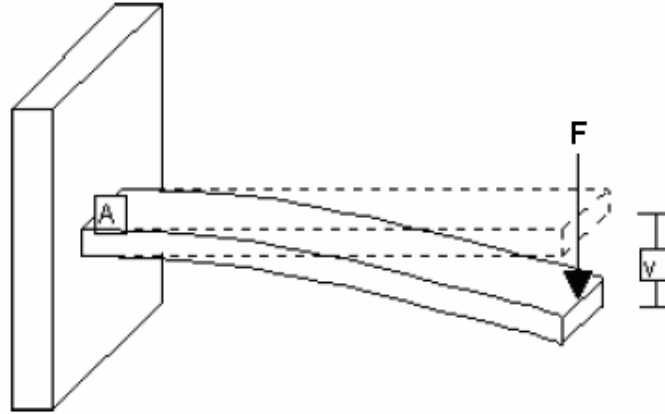


**Figure 3.24:** The Cantilever Beam Deflection Under Force at the Free End [15]

Force “ $F$ ” can be expressed as:

$$F = -kx \quad (3.17)$$

where “ $k$ ” is the spring constant of the cantilever beam and “ $x$ ” is the deflection under applied voltage. The curvature of the beam  $\kappa$  is equal to the second derivative of the tip deflection [15]:

$$\kappa = \frac{\partial^2 v(x)}{\partial x^2} \quad (3.18)$$

The curvature can also be related to bending moment  $M$  and the flexural rigidity  $EI$  [15]:

$$\kappa = \frac{M}{EI} \quad (3.19)$$

The bending moment can be related to the shear force  $S$ , and the lateral load  $q$  on the beam [15]. Thus,

$$M = EI \frac{\partial^2 v(x)}{\partial x^2} \quad (3.20)$$

$$S = EI \frac{\partial^3 v(x)}{\partial x^3} \quad (3.21)$$

$$q = -EI \frac{\partial^4 v(x)}{\partial x^4} \quad (3.22)$$

For the force shown in Figure 3.24, according to the reference [15], the distributed load, shear force, and bending moment are:

$$q(x) = 0 \quad (3.23)$$

$$S(x) = F \quad (3.24)$$

$$M(x) = -Fl\left(1 - \frac{x}{l}\right) \quad (3.25)$$

Thus, according to the reference [15] the solution of Eq. (3.20) is

$$\frac{\partial v(x)}{\partial x} = \int_{x=0}^x M(x) dx = -\frac{Fl}{EI} \left( x - \frac{x^2}{2l} \right) \quad (3.26)$$

$$v(x) = \int_{x=0}^x \frac{\partial v(x)}{\partial x} dx = -\frac{Fl}{EI} \left( \frac{x^2}{2} - \frac{x^3}{6l} \right) \quad (3.27)$$

And at the free end of the beam, the displacement is

$$v(L) = -\frac{Fl^3}{3EI} \quad (3.28)$$

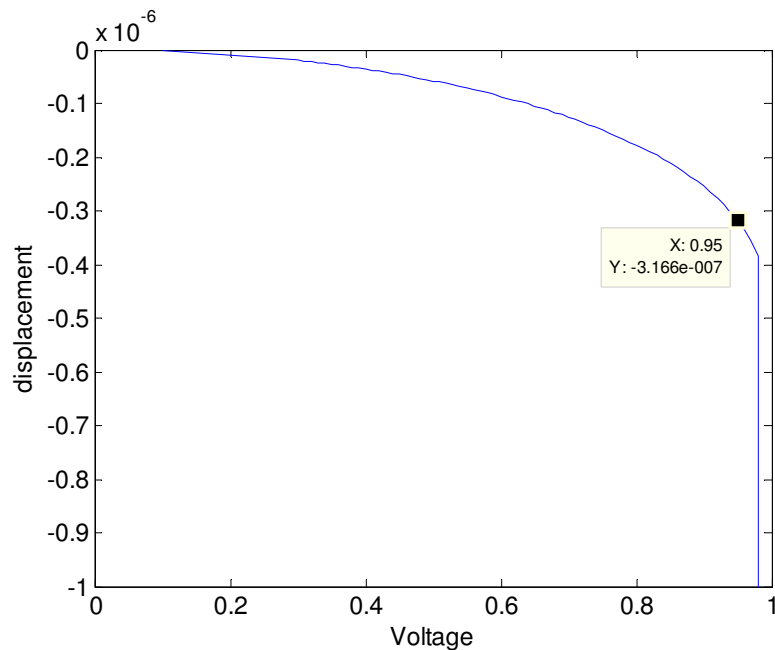


**Figure 3.25:** The Displacement for  $l=260\mu\text{m}$ ,  $w=50\mu\text{m}$ ,  $d_0=1\mu\text{m}$ , and  $h=1\mu\text{m}$

The force “F” will be obtained from the displacement occurred due to the voltage while there is no vibration. We know that for  $l= 260\mu\text{m}$ ,  $w=50 \mu\text{m}$ ,  $d_0=1 \mu\text{m}$ , and  $h=1 \mu\text{m}$ , the displacement is like as in the Figure 3.25.

At this condition, the pull-in voltage is 0.98 Volt. We can choose 0.95 Volt for our analysis. By using data cursor, we can see that the deflection at 0.95 Volt is  $-0.3166 \mu\text{m}$ . The spring constant of the beam is,

$$k = \frac{E_{eff} wh^3}{4l^3} \quad (3.29)$$

where  $E_{eff}$  is the effective modulus of the beam. For  $l= 260\mu\text{m}$ ,  $w=50 \mu\text{m}$ ,  $d_0=1 \mu\text{m}$ , and  $h=1 \mu\text{m}$ , the force is,

$$F = -kx = -(0.1005)(-0.3166 \times 10^{-6}) = 3.1821 \times 10^{-8} \text{ N} \quad (3.30)$$

At this condition, the tip deflection at the free end of the beam becomes,

$$v(L) = -\frac{Fl^3}{3EI} = -0.31665 \times 10^{-6} \quad (3.31)$$

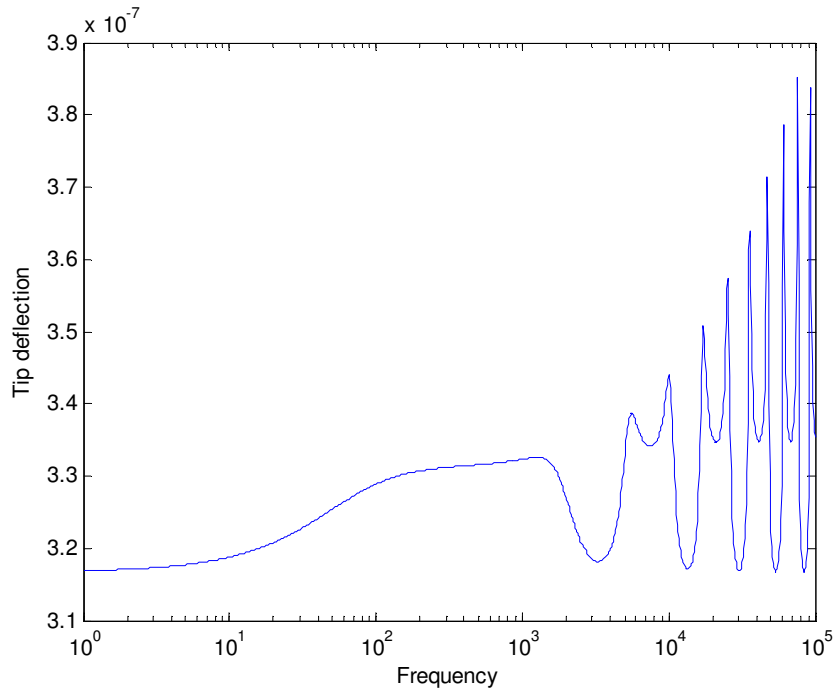


**Figure 3.26:** The Tip Deflection of The Beam When The Base Displacement is  $100\mu\text{m}$  at 200 Hz for  $l=260\mu\text{m}$ ,  $w=50 \mu\text{m}$ ,  $d_0=1 \mu\text{m}$ , and  $h=1 \mu\text{m}$  and Voltage is 0.95 Volt

It is logical that the tip deflection is approximately equal to the deflection of the beam. Then, as we have mentioned before, using super position method, adding each deflection of both cases can give the tip deflection while there are a vibration and an applied voltage to the beam. For  $l=260\mu\text{m}$ ,  $w=50\mu\text{m}$ ,  $d_0=1\mu\text{m}$ , and  $h=1\mu\text{m}$ , the tip deflection under 0.95 Volt and a vibration having  $100\times 10^{-6}$  amplitude and 200 Hz frequency can be seen in the Figure 3.26. Also, we can see the tip deflection changes for different amplitudes of vibration in the Figure 3.27.

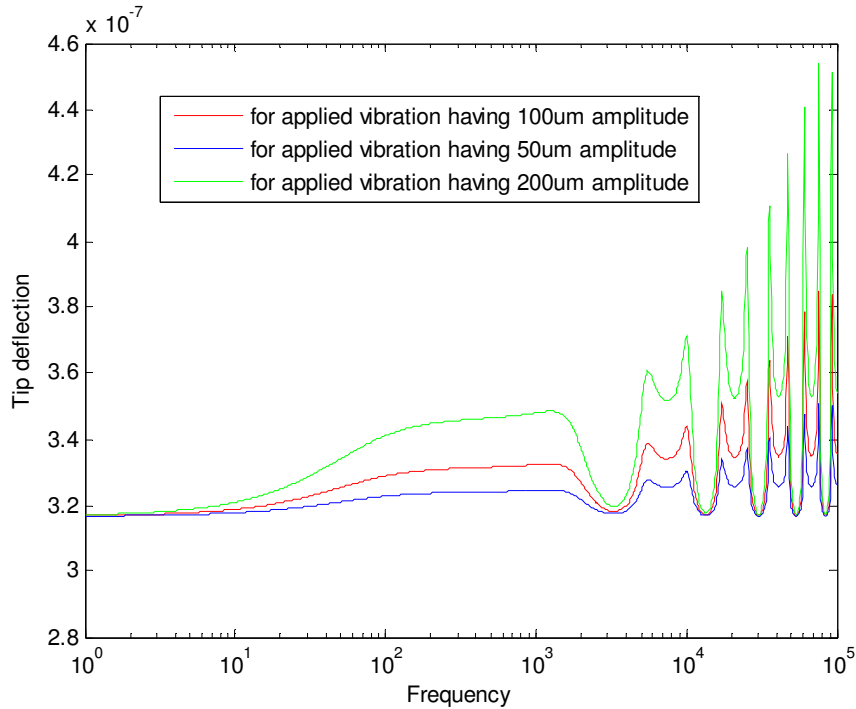


**Figure 3.27:** The Tip Deflection Change for Different Amplitudes of Vibration and for 0.95 Volt

Observing the figures, we can say that when a vibration affects at the base of the cantilever beam that has  $100\mu\text{m}$  amplitude and  $200\text{Hz}$  frequency while the voltage is 0.95 Volt, the tip deflection is  $0.3307\mu\text{m}$ . This result is good as the tip deflection is less than pull-in gap, although it is the worst case for our design.

If we want to see how the pull-in changes that when a vibration affects at the base of the cantilever beam that has  $100\mu\text{m}$  amplitude and  $200\text{Hz}$  frequency under increasing voltage by using Comsol, we must take  $F$  that is the force caused by the tip deflection when only vibration affects the beam and its change due to the frequency can be seen in the Figure 3.28. At this force expression, the value that we are interested is the force at 200 Hz that is  $F=1.412\times 10^{-9}$  N. Putting this value to our simulation on

Comsol, we can obtain the pull-in graph as in the Figure 3.29 with comparison to pull-in graph without vibration for  $l=260\mu\text{m}$ ,  $w=50\mu\text{m}$ ,  $d_0=1\mu\text{m}$ , and  $h=1\mu\text{m}$ .

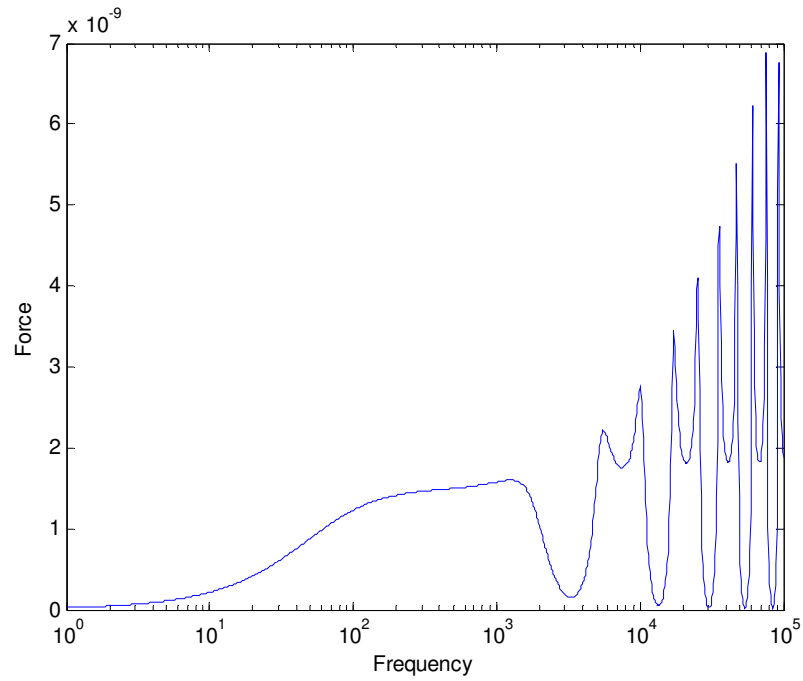


**Figure 3.28:** The Force Caused by the Tip Deflection When Only Vibration Affects the Beam

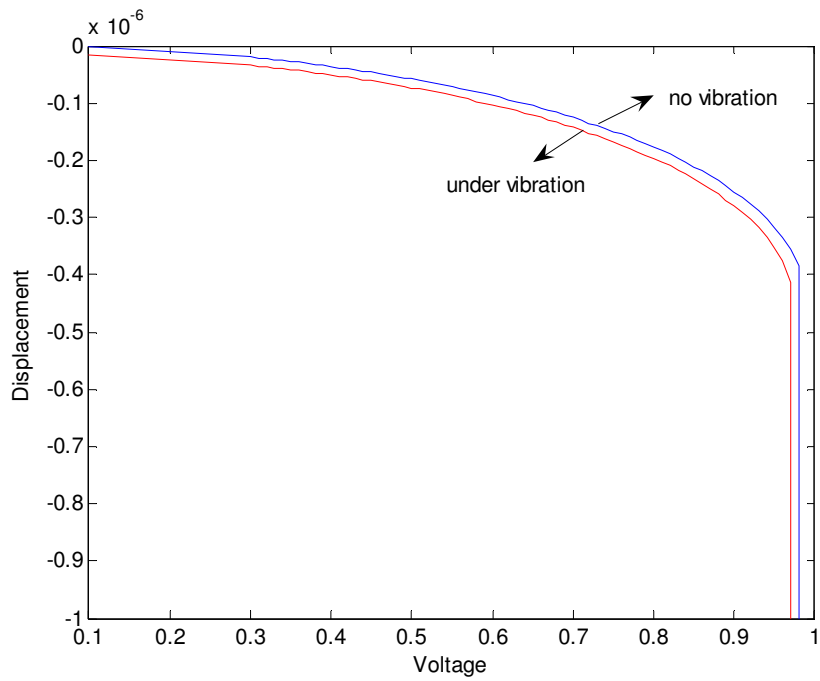


**Figure 3.29:** The Comparison of the Displacement Without a Vibration and Under Vibration That Has a Force  $F=1.412 \times 10^{-9}$  N at The Free End of the Beam

It is clear that there is not more difference between two conditions. Thus, vibration does not affect deflection and pull-in voltage so much. This result is prominent for our design as it indicates that our design sizes are robust under a vibration having  $100 \times 10^{-6}$  amplitude and 200 Hz frequency if we produce the beam from Polysilicon. Under this vibration the pull-in voltage becomes 0.97 Volt while the pull-in voltage is 0.98 Volt under no vibration.

If want to produce the beam from Aluminum, we know that under no vibration the pull-in voltage is approximately 0.73 Volt. Assuming applied voltage is 0.7 volt and a vibration affecting the base of the beam has  $100 \mu\text{m}$  amplitude and 200Hz frequency, the tip deflection of the cantilever beam becomes as in the Figure 3.30.

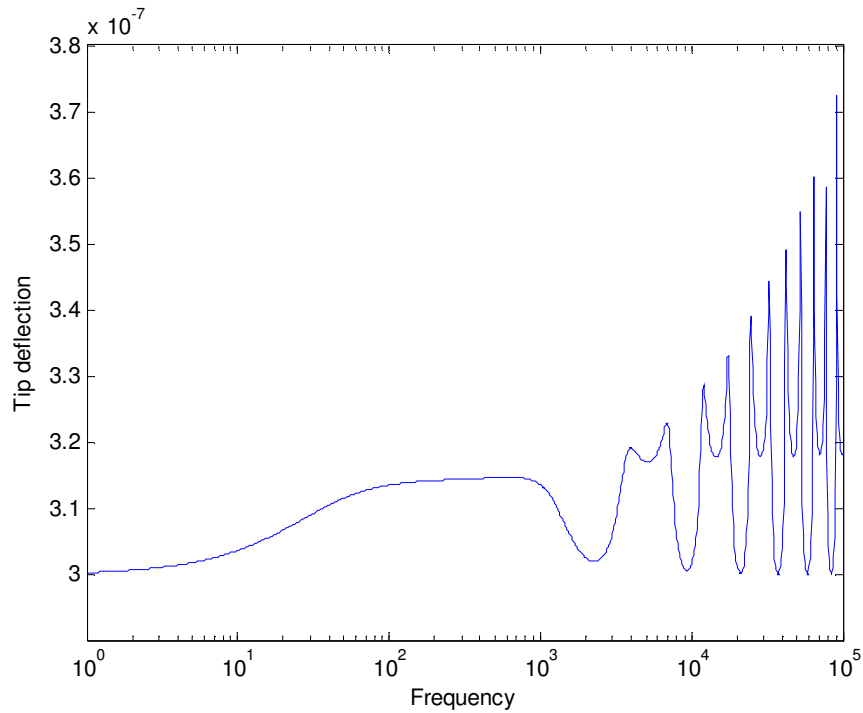


**Figure 3.30:** The Tip Deflection of the Beam Made of Aluminum When the Base Displacement is  $100 \mu\text{m}$  at 200 Hz for  $l=260 \mu\text{m}$ ,  $w=50 \mu\text{m}$ ,  $d_0=1 \mu\text{m}$ , and  $h=1 \mu\text{m}$  and Voltage is 0.7 Volt

Observing the figure, we can say that when a vibration affects the base of the cantilever beam that has  $100 \mu\text{m}$  amplitude and 200 Hz frequency while the voltage is 0.7 Volt, the tip deflection is  $0.3141 \mu\text{m}$ . This result is so good since the tip deflection is less than pull-in gap, although it is the worst case for our design. If we want to see how the pull-in changes that when a vibration affects at the base of the cantilever beam that has  $100 \mu\text{m}$  amplitude and 200 Hz frequency under increasing

voltage by using Comsol, we must take  $F$  that is the force caused by the tip deflection when only vibration affects the beam and its change due to the frequency can be seen in the Figure 3.31. At this force expression, the value that we are interested is the force at 200 Hz that is  $F= 8.013 \times 10^{-10}$  N. Putting this value to our simulation on Comsol, we can obtain the pull-in graph as in the Figure 3.32 with comparison to pull-in graph without vibration for  $l= 260 \mu\text{m}$ ,  $w=50 \mu\text{m}$ ,  $d_0=1 \mu\text{m}$ , and  $h=1 \mu\text{m}$ .

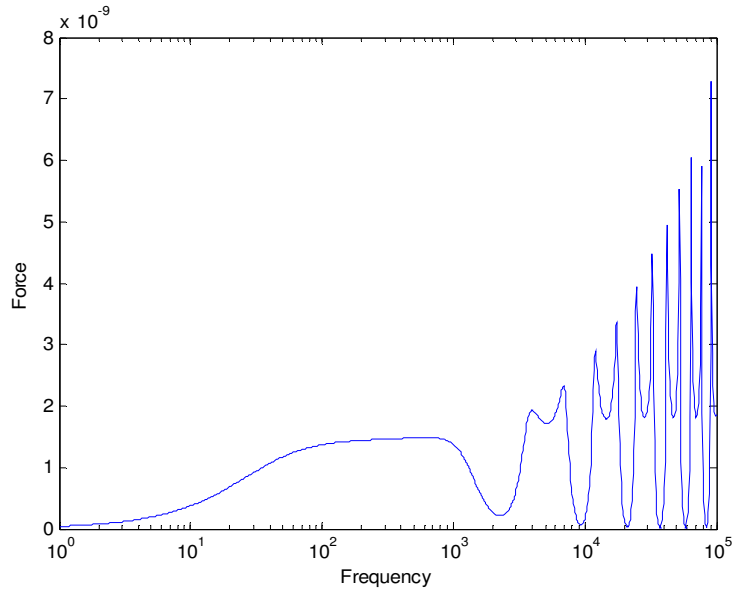


**Figure 3.31:** The Force Caused by the Tip Deflection When Only Vibration Affects the Beam Made of Aluminum

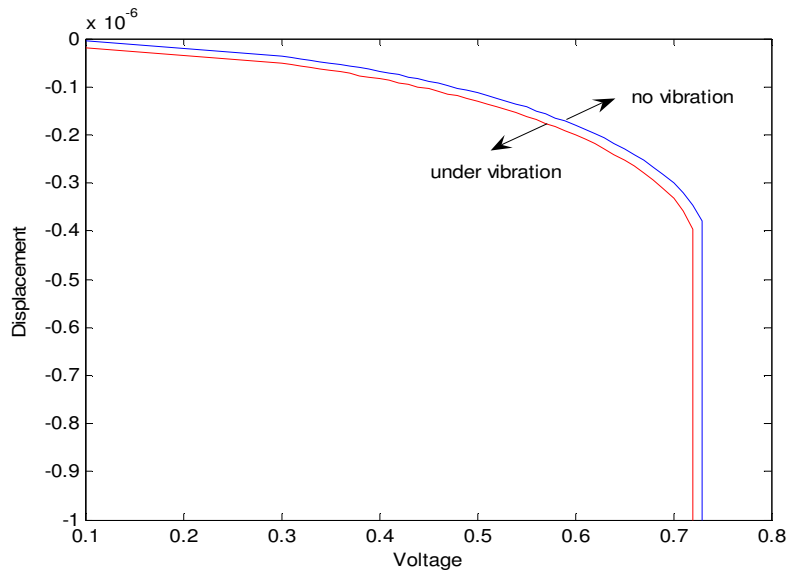


**Figure 3.32:** The Comparison of the Displacement Without a Vibration and Under Vibration that has a Force  $F= 8.013 \times 10^{-10}$  N at the Free End of the Beam Made of Aluminum

It can be said that the vibration does not make more difference between two conditions for a cantilever beam made of Aluminum. Under this vibration the pull-in voltage becomes 0.72 Volt while the pull-in voltage is 0.73 Volt under no vibration.

As we know, under no vibration the pull-in voltage for a cantilever beam made of Gold is 0.77 Volt. Assuming that while applied voltage is 0.73, a vibration affects the base of the cantilever beam that has 100 $\mu\text{m}$  amplitude and 200 Hz frequency, the tip deflection can be seen in Figure 3.33. The figure shows that when a vibration affects at the base of the cantilever beam that has 100 $\mu\text{m}$  amplitude and 200 Hz frequency while the voltage is 0.73 Volt, the tip deflection is 0.3061  $\mu\text{m}$ . This value is convenient for our design as it is less than the pull-in gap. It can be useful to see how the pull-in changes that when a vibration affects at the base of the cantilever beam that has 100 $\mu\text{m}$  amplitude and 200 Hz frequency under increasing voltage by using Comsol, we must take F that is the force caused by the tip deflection when only vibration affects the beam and its change due to the frequency can be seen in the Figure 3.34. At this force expression, the value that we are interested is the force at 200 Hz that is  $F= 1.041 \times 10^{-9}$  N. Putting this value to our simulation on Comsol, we can obtain the pull-in graph as in the Figure 3.35 with comparison to pull-in graph without vibration for  $l= 260\mu\text{m}$ ,  $w=50\mu\text{m}$ ,  $d_0=1\mu\text{m}$ , and  $h=1\mu\text{m}$ .

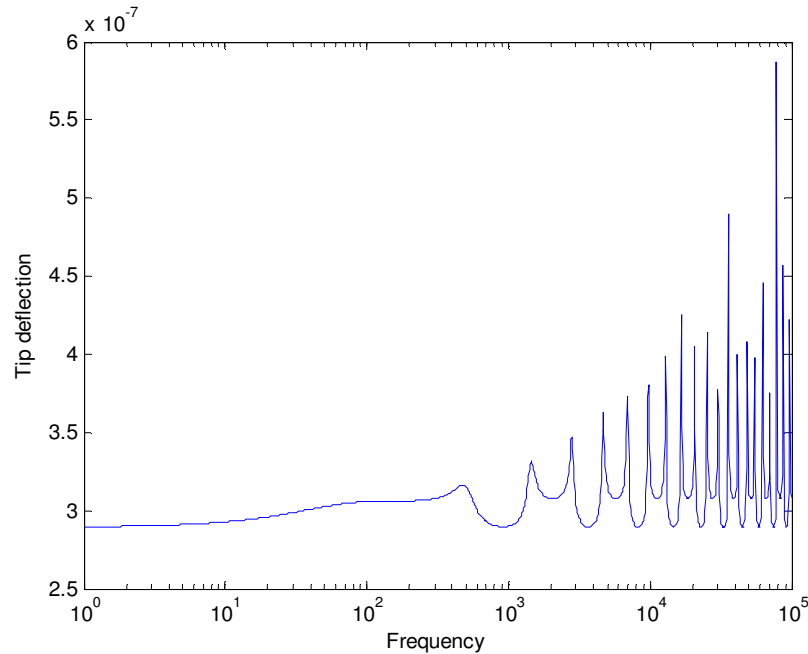


**Figure 3.33:** The Tip Deflection of the Beam Made of Gold When the Base Displacement is 100 $\mu\text{m}$  at 200 Hz for  $l=260\mu\text{m}$ ,  $w=50\mu\text{m}$ ,  $d_0=1\mu\text{m}$ , and  $h=1\mu\text{m}$  and Voltage is 0.73 Volt

As it can be seen in the Figure 3.35, there exists no more difference between two conditions for a cantilever beam made of Gold. Under this vibration the pull-in voltage becomes 0.76 Volt while the pull-in voltage is 0.77 Volt under no vibration.

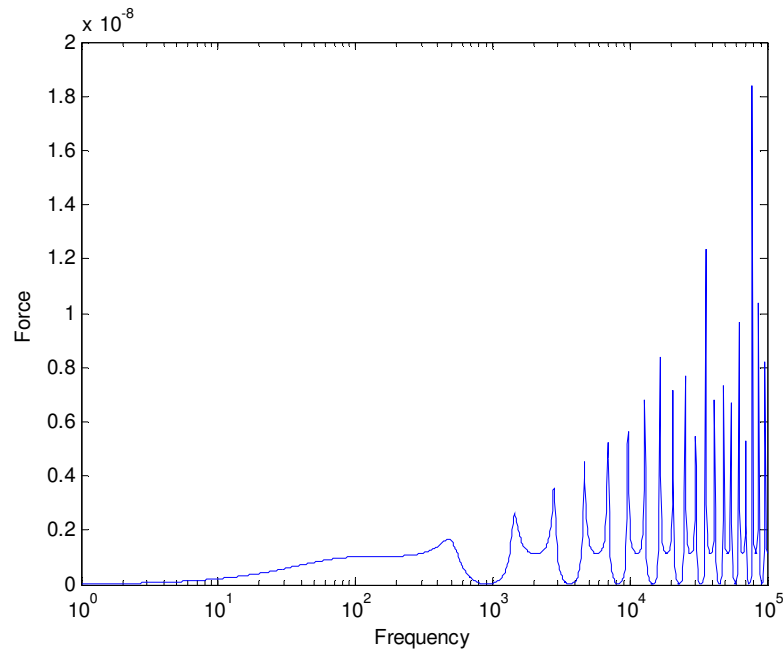


**Figure 3.34:** The Force Caused by the Tip Deflection When Only Vibration Affects the Beam Made of Gold

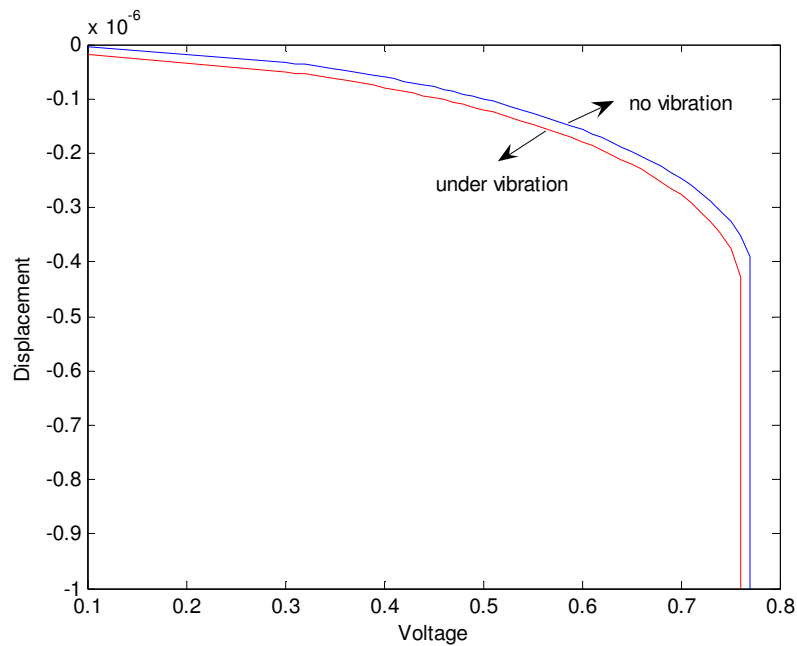


**Figure 3.35:** The Comparison of the Displacement Without a Vibration and Under Vibration that has a Force  $F= 1.041 \times 10^{-9}$  N at the Free End of the Beam Made of Gold

Regarding to the tip deflection results and the pull-in voltage results for different materials under a vibration, it can be said that it does not make so difference to produce the cantilever beam from Polysilicon, Aluminum or Gold. All results demonstrate that our design sizes are robust under a vibration having 100 $\mu$ m amplitude and 200 Hz frequency even if we produce the beam from Polysilicon, Aluminum or Gold. The percentage of pull-in point changes for different materials can be seen in Table 3.7. The minimum percentage change is for a cantilever beam made of Polysilicon and the maximum is for a cantilever beam made of Aluminum. Thus, it may be advantageous to produce the cantilever beam from Polysilicon.

**Table 3.7:** The Comparison of Pull-in Point Changes for Conditions Under Vibration and No Vibration

<b>Cantilever Beam</b>	<b>Pull-in Voltage (No Vibration)</b>	<b>Pull-in Voltage (Vibration at 200Hz with 100 <math>\mu</math>m amplitude)</b>	<b>Percentage of Pull-in Voltage Change</b>
Polysilicon	0.98 Volt	0.97 Volt	% 1
Aluminum	0.73 Volt	0.72 Volt	% 1.37
Gold	0.77 Volt	0.76 Volt	% 1.30

### 3.6 Damping Factor and Response to Accelerations

**Table 3.8:** Common Sources of Vibrations [17]

<b>Vibration Source</b>	<b>Frequency of Peak (Hz)</b>	<b>Peak Acceleration (<math>m/s^2</math>)</b>
Kitchen Blender Casing	121	6.4
Clothes Dryer	121	3.5
Door Frame (just after door closes)	125	3
Small Microwave Oven	121	2.25
HVAC Vents in Office Building	60	0.2-1.5
Bread Maker	121	1.03
External Windows (size 2ftx3ft) next to a busy street	100	0.7
Notebook Computer while CD is being read	75	0.6
Washing Machine	109	0.5
Refrigerator	240	0.1

One of the ultimate goals of designing a cantilever beam is to check the responses of step accelerations affecting the base of the beam. In this analysis, we get “g” as the acceleration of the gravity whose value is  $10 \text{ m/s}^2$ . Observing the step responses of the beam for different values of acceleration and damping constant is so valuable for our design. Then, the designer can decide whether the beam is robust under different accelerations, or not, and obtain the critical damping constant value that cause an overshoot in the step response of the beam. In this analysis, peak values of vibrations should be taken into consideration after reviewing common sources of vibrations as in Table 3.8 [17]. Peak accelerations of vibrations sources are assumed in the range of 0-10g. Also, response of the cantilever beam under crash effects will be examined.

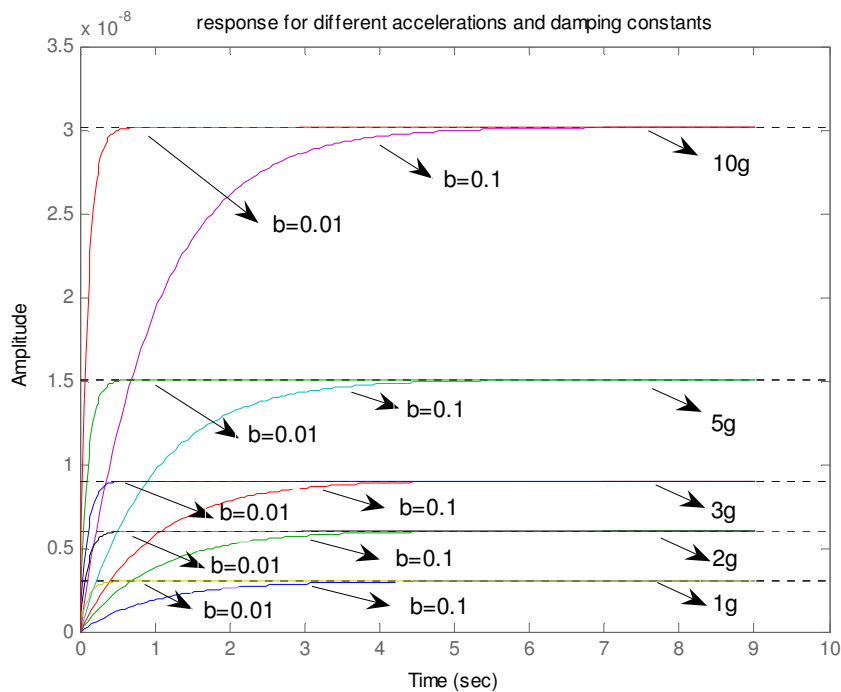


**Figure 3.36:** The Step Responses for Different Values of Acceleration and Damping Constant for a Cantilever Beam Made of Polysilicon

First of all, this analysis will be applied to the cantilever beam made of Polysilicon whose optimum sizes have been obtained in the previous parts of this study. The step responses for different values of acceleration and damping constant for the optimum sizes of  $l=260\mu\text{m}$ ,  $w=50\mu\text{m}$ ,  $d_0=1\mu\text{m}$ , and  $h=1\mu\text{m}$  can be seen in the Figure 3.36. A decrease in the value of damping constant only makes a decrease in the value of step response time. Also, increasing the acceleration value only increases the settling

value of step response. Changing the value of the damping constant does not affect the settling value. The settling value of the beam for 10g is approximately 0.03  $\mu\text{m}$  which is so good for our design.

To obtain the critical damping constant value, the damping ratio should be considered. Assuming the beam will make 3% overshoot, from Eq. (3.32) where  $M_p$  is the maximum value of the step response, the critical damping ratio can be obtained.

$$\zeta = \sqrt{\frac{[\ln(M_p - 1)]^2}{\pi^2 + [\ln(M_p - 1)]^2}} \quad (3.32)$$

Obtaining the critical damping ratio, using Eq. (3.33) where “k” is spring constant of the beam and “m” is the mass of the beam, the critical damping constant “b” can be calculated.

$$\zeta = \frac{b}{2\sqrt{km}} \quad (3.33)$$

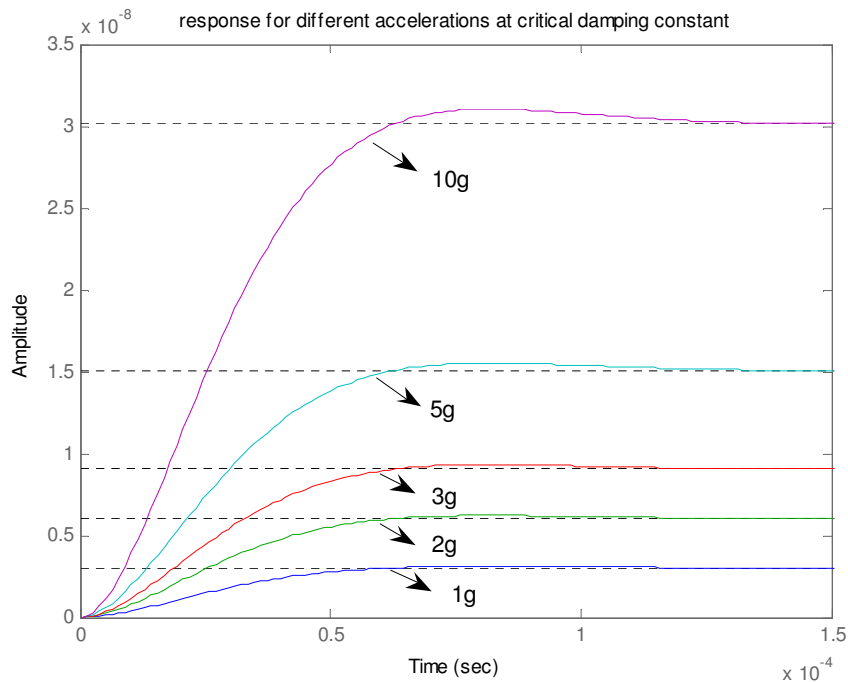


**Figure 3.37:** The Step Responses for Different Values of Acceleration at Critical Damping Constant for a Cantilever Beam Made of Polysilicon

For optimum design values, the critical damping constant for the cantilever beam made of Polysilicon becomes  $2.598 \times 10^{-6}$  Ns/m. For this value, the step responses for different accelerations can be seen in Figure 3.37. This result indicates that values of damping constant less than the critical damping constant value cause an overshoot in the step response of the beam. Thus, while designing a cantilever beam from Polysilicon for our optimum values this critical damping constant value should be considered.

It is so useful to obtain the critical damping constant values for cantilever beam made of different materials. At first, assuming the beam will make 3% overshoot, for optimum design values, the critical damping constant for the cantilever beam made of Aluminum becomes  $2.086 \times 10^{-6}$  Ns/m. For this value, the step responses for different accelerations can be seen in Figure 3.38. This result also indicates that values of damping constant less than the critical damping constant value cause an overshoot in the step response of the beam. Thus, while designing a cantilever beam from aluminum for our optimum values this critical damping constant value should be considered. Furthermore, the settling value of the beam for 10g is approximately  $0.021 \mu\text{m}$  that is convenient for our design.

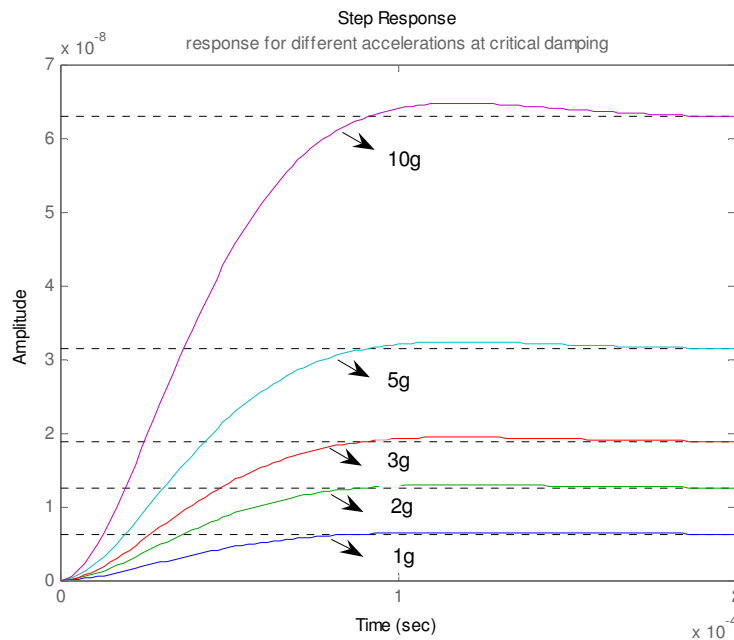


**Figure 3.38:** The Step Responses for Different Values of Acceleration at Critical Damping Constant for a Cantilever Beam Made of Aluminum

After the analysis for Aluminum, applying the same one for the cantilever beam made of Gold can be so useful to compare the results of the analysis for different materials. Assuming the beam will make 3% overshoot, for optimum design values, the critical damping constant for the cantilever beam made of Gold becomes  $5.862 \times 10^{-6}$  Ns/m. For this value, the step responses for different accelerations can be seen in Figure 3.39. This result also indicates that while designing a cantilever beam from gold for our optimum values, designer should consider that values of damping constant less than the critical damping constant value cause an overshoot in the step response of the beam. Furthermore, the settling value of the beam for 10g is approximately  $0.36 \mu\text{m}$  that is not convenient for our design.

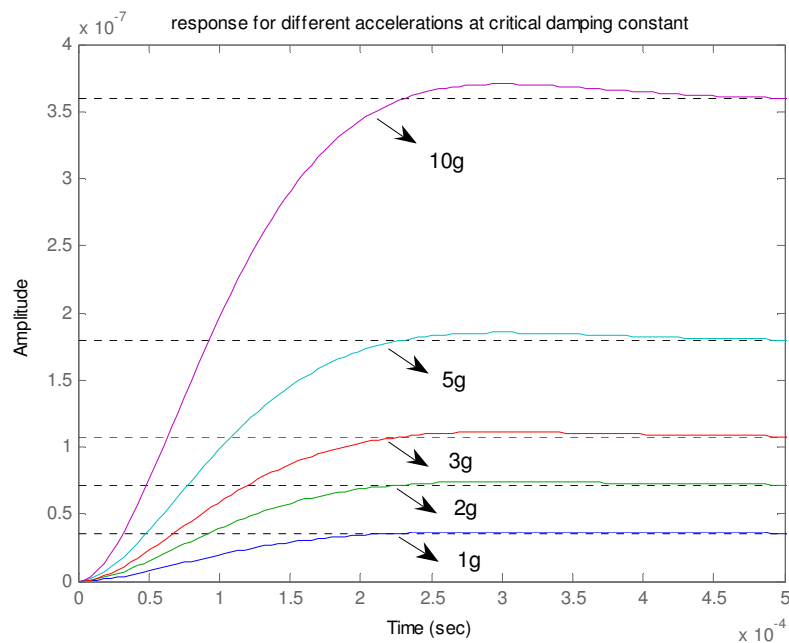


**Figure 3.39:** The Step Responses for Different Values of Acceleration at Critical Damping Constant for a Cantilever Beam Made of Gold

The different results for different design considerations can be used to make a comparison table like Table 3.9. As it can be seen, assuming that maximum 10g acceleration affects the base of the beam, the worst result is for the cantilever beam made of gold and the best results are for the cantilever beams made of aluminum and Polysilicon. Considering one of the main goals of designing our cantilever beam that is to make it robust under step accelerations, making the cantilever beam from Polysilicon or aluminum is so advantageous not only for critical damping value but also for maximum deflection at these accelerations.

**Table 3.9:** The Comparison of Critical Damping Constants and Deflections at 10g for Different Cantilever Beams

Cantilever Beam	Polysilicon	Aluminum	Gold
<b>Critical Damping Constant</b>	$2.598 \times 10^{-6}$ Ns/m	$2.086 \times 10^{-6}$ Ns/m	$5.862 \times 10^{-6}$ Ns/m
<b>Maximum Deflection at 10g Acceleration</b>	0.03 $\mu\text{m}$	0.062 $\mu\text{m}$	0.36 $\mu\text{m}$

Assume that power harvesting device is used in packaging industry and one of the regarding packages drops to the ground from one meter. In mechanical analysis of the crash of two rigid materials, the simulation time is taken as 10ms. The package has a velocity as 4,4m/s when it reaches to the ground. Thus, instant acceleration occurred on the package can be calculated as approximately 44g. Considering the errors, we can make simulations for 50g. Related to the previous results, we can make simulation to see responses of cantilever beams made of Polysilicon and Aluminum to an instant acceleration, so it is unnecessary to make simulations for other cases. Looking the results as in Figure 3.40 and considering the worst cases, under accelerations the most suitable design is Polysilicon cantilever beam.

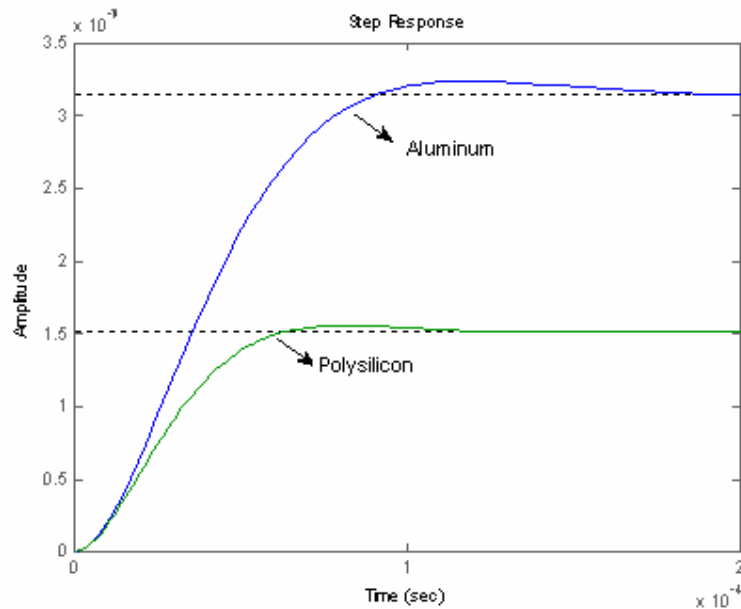


**Figure 3.40:** The Responses of Polysilicon and Aluminum Cantilever Beams Under 50g Acceleration

Acceleration is either a short-time and fast varying effect or a changing effect. It can not be constant over a long period. Therefore, after acceleration signal, the beam oscillates and settles down its zero position [10]. For a spring mass system as in Figure 3.2, the balanced position of the mass is taken as  $x=0$ . If the effect of damping is considered, the oscillation will finish and the mass will eventually settle at  $x=x_0$  when the energy is completely consumed by the damping. Thus, the response of the system to a step acceleration or force is strongly dependent on the damping. Other characteristics of the system like stiffness do not affect the step response. Decreasing the stiffness of the beam does not affect the maximum deflection of the beam and oscillation [10]. The response of the beam made of Polysilicon to 10g step acceleration for different damping ratios can be observed in Figure 3.41. It is clear that if the beam is required not to make more oscillation, the damping ratio should be settled around 0.7 values.

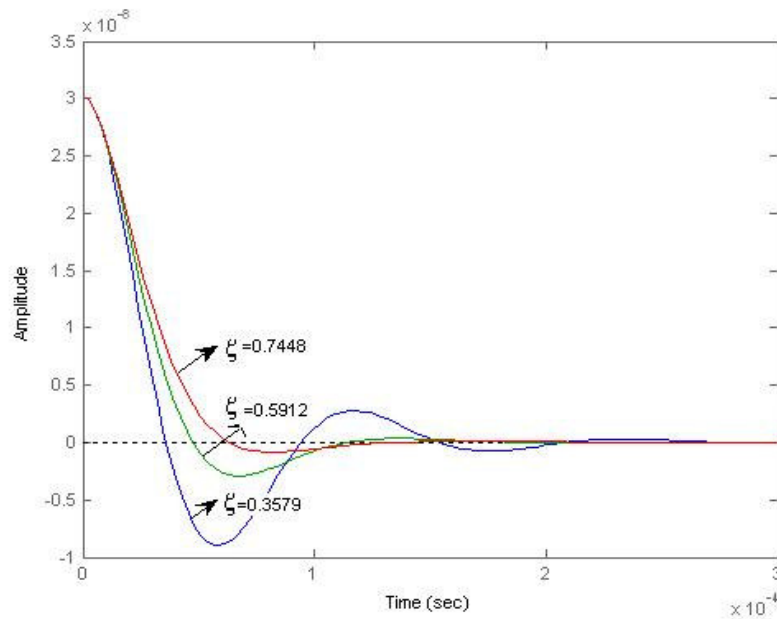


**Figure 3.41:** The Response of the Beam Made of Polysilicon to 10g Step Acceleration for Different Damping Ratios

### 3.7 Hysteresis and Resistance Considerations

Lots of the electrostatic actuators can be modeled as a mobile plate attached to a spring as in the Figure 3.42 [18]. At equilibrium voltage  $V=0$  and capacitor gap is  $g$  ( $z=0$ ). The capacitor formula is [18]

$$c = \frac{\epsilon_0 S}{(g - z)} \quad (3.35)$$

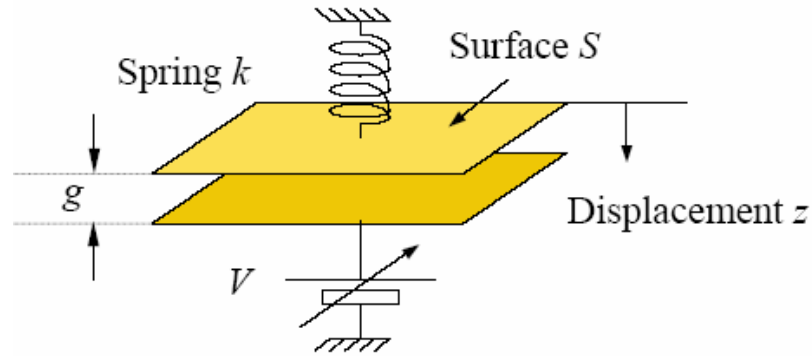


**Figure 3.42:** Model of an Electrostatic Actuator [18]

When a voltage  $V$  is applied, the electrostatic force causes the reduction of the capacitor gap and the spring force induced by the plate displacement tends to counteract the electrostatic force effects. Eq. (3.36) gives the electrostatic force and Eq. (3.37) gives spring force [2].

$$F_{el} = \frac{1}{2} V^2 \frac{\epsilon_0 S}{(g - z)^2} \quad (3.36)$$

$$F_{sp} = -kz \quad (3.37)$$

The equilibrium graph can be seen in Figure 3.43 [18] and the equilibrium position  $z$  of the plate versus  $V$  voltage is given by,

$$F_{el} + F_{sp} = 0 \quad (3.38)$$

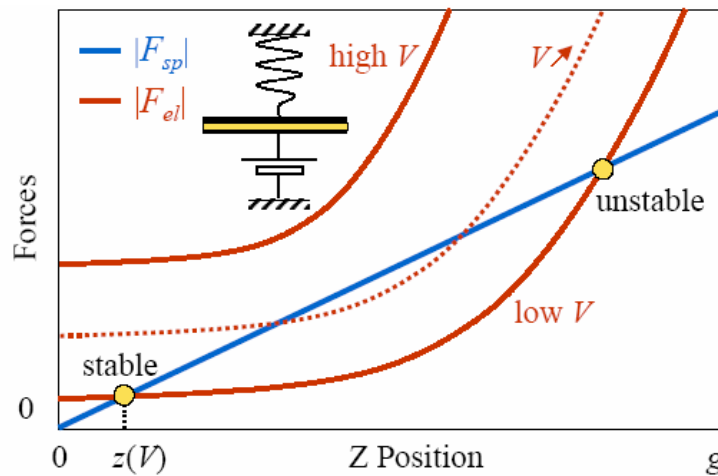


**Figure 3.43:** The Equilibrium Graph [18]

At low voltage there are two equilibrium positions. One is stable the other is unstable. At higher voltage there is no more equilibrium position. The electrostatic force is always greater than the spring force: the mobile plate is pulled down to the fixed plate. This effect is called as pull-in effect and occurs for a voltage greater than the pull-in voltage  $V_{pull-in}$ . Note that for this type of electrostatic actuator it is necessary to insulate the two plates to avoid electrical short circuit when the pull-in effect occurs [2].

Equilibrium positions and pull-in voltage are deduced from the equation  $F_{el} + F_{sp} = 0$ , which leads to the Figure 3.44 [18]. Stable equilibrium positions exist only in the region  $0 < z < g/3$ . The pull-in voltage is calculated at the limit of the stable region [18]:

$$\frac{\epsilon_0 S}{2k} V_{pull-in}^2 = \frac{4}{27} g^3 \quad (3.39)$$

$$V_{pull-in} = \sqrt{\frac{8kg^3}{27\epsilon_0 S}} \quad (3.40)$$

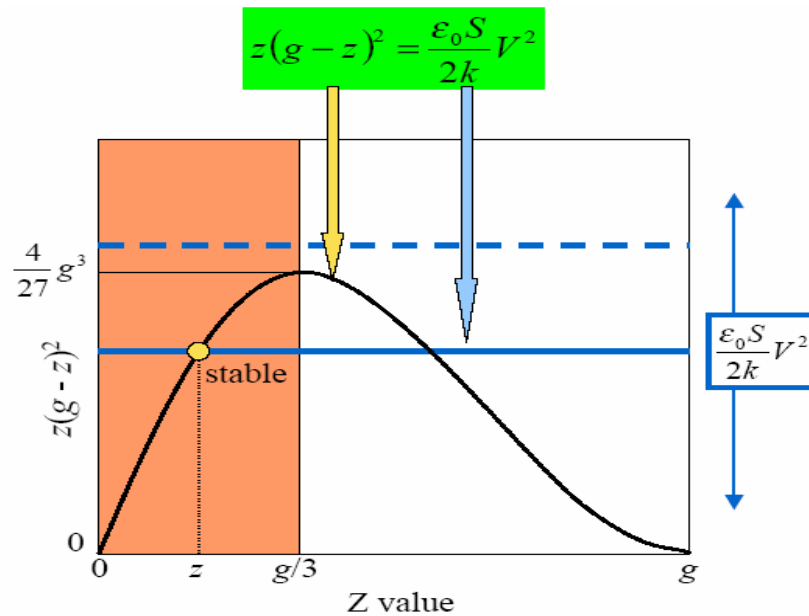


**Figure 3.44:** The Graph Led by  $F_{el} + F_{sp} = 0$  Deduces Equilibrium Positions and Pull-in Voltage [18]

When the pull-in effect occurs, the mobile plate is pulled down to the insulator layer of the fixed plate. As the plate gap is very small, the electrostatic force is very large, much more important than the spring force. The voltage has to be reduced to allow

the separation of the two plates, which is called the pull-out voltage. The pull-out situation is illustrated in the Figure 3.45 [18]. Below the pull-out voltage the spring force becomes larger than the electrostatic force at closed gap and can separate the two plates. From the equilibrium of the forces, the pull-out voltage can be obtained as [18]:

$$\frac{1}{2}V_{pull-out}^2 \frac{\epsilon_0 \epsilon_x S}{t_{ox}^2} = kg \quad (3.41)$$

$$V_{pull-out} = \sqrt{\frac{2kgt_{ox}^2}{\epsilon_0 \epsilon_x S}} \quad (3.42)$$

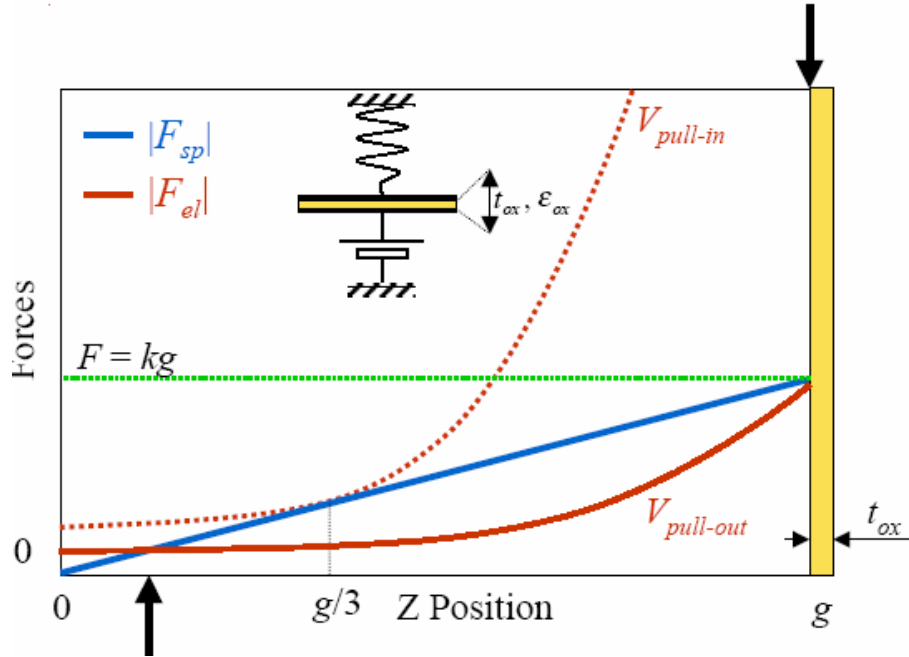


**Figure 3.45:** The Graph of the Pull-out Situation [18]

The changes in the applied voltage causes a hysteresis for the actuator as illustrated in Figure 3.46 [18]. At the first region the voltage increases and the mobile plate moves down. At the end of the second region pull-in occurs. When the voltage is reduced, pull-out occurs at the end of the third region. These events bring a hysteresis cycle for an electrostatic actuator.

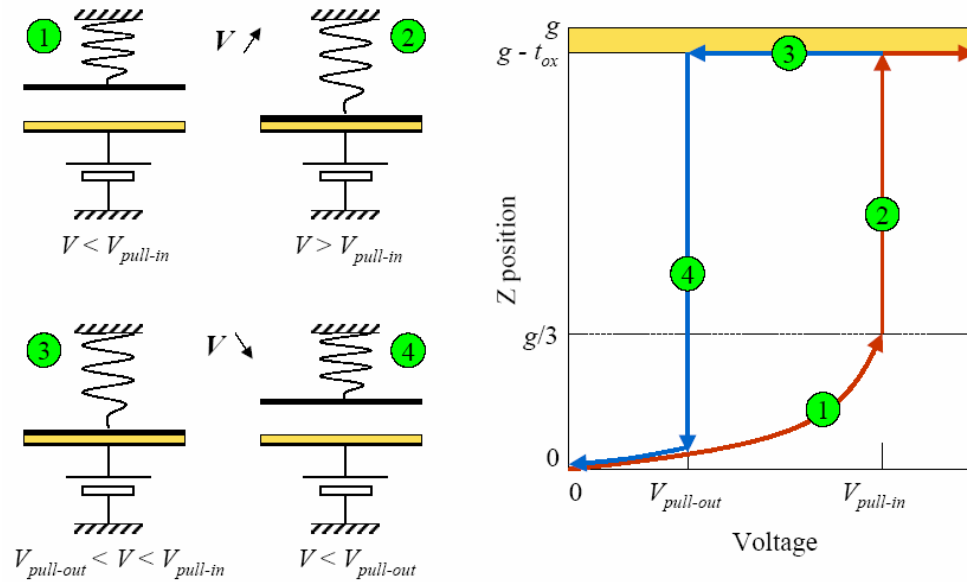


**Figure 3.46:** The Illustration of the Hysteresis Cycle [18]

All information given above is valid for cantilever beams having a dielectric space on the ground plane. However, the cantilever beam that is required for our system does not contain any dielectric space. Also, there is no model in the literature for the type of cantilever beams we are interested in. We know the point where our cantilever beam pulls in, but it is uncertain at which voltage our cantilever beam pulls out. Thus, we can give an estimation or percentage between pull-in and pull-out voltages by observing studies and experiments that have been examined in previous papers.

The cantilever beam we are concerned can be seen as a micro relay, so we can take papers that studied the micro relays into consideration. A micro relay has been designed in [19]. In this paper, the relay demonstrates hysteresis and pulls down at 82V and pulls up at around 76V, which gives a ratio between pull-up and pull-down that is approximately 0.92. Also, micromechanical relays have been examined in [20]. In this article, for a constant voltage applied on the working port, the measured pull-in voltage can be taken as 44.5V and the measured pull-out voltage can be taken as 40V, that gives the ratio between pull-out and pull-in that is 0.89. In other paper that is [21], the pull-in and pull-out voltages of some micro actuators have been analyzed regarding to the hysteresis. In this analysis, a stopper has been used to limit the displacement of the movable part, not the cause of the hysteresis, only determines the hysteresis magnitude. The experimental results of this article shows that for the

asymmetrically designed micro actuator the ratio between the pull-out and pull-in voltages is approximately 0.98 and for the symmetrically designed micro actuator the ratio is around 0.85. Observed information from these papers can be seen in Table 3.10.

**Table 3.10:** Observed Information from Some Papers

	$V_{\text{pull-in}}$	$V_{\text{pull-out}}$	$V_{\text{pull-out}} / V_{\text{pull-in}}$
<b>Paper [19]</b>	82V	76V	0.92
<b>Paper [20]</b>	44.5V	40V	0.89
<b>Paper [21] (asymmetrically)</b>	9.34V	9.27V	0.98
<b>Paper [21] (symmetrically)</b>	11.89V	10.15V	0.85

Furthermore, electro-statically actuated micromechanical switches have been examined in [22]. This paper indicates that if the contact resistance is very high, the micro switches pull out at nearly the same voltage at which they pull in. Also, it adds that when the contact resistance is small, the pull-out voltage becomes smaller- indicating the existence of adhesive forces which tend to hold the switches closed. All results gathered from different papers conclude that to make the hysteresis possible we should make the contact resistance of our cantilever beam relatively small. Modeling contact resistance has 3 steps: finding the contact force as a function of applied voltage, finding contact area as a function of the contact force, and calculating the contact resistance as a function of the contact area [22]. Thus, the pull-in and pull-out voltages will be different and the pull-out voltage of our cantilever beam may be assumed as in the region 80% of  $V_{\text{pull-in}} \leq V_{\text{pull-out}} \leq 98\%$  of  $V_{\text{pull-in}}$ .

The situation of the whole system for on and off positions of the switch can be seen in Figure 3.47. At this condition, calculating the resistance of cantilever beams made of Polysilicon, Aluminum, and Gold brings useful information for electrical properties of power harvesting system. It is required that the resistance of the switch should be higher than assumed equivalent resistance of the circuit. We want that the current on the circuit must be approximately 10 $\mu$ A. Thus, if the applied voltage is 1V, equivalent resistance of the circuit is required to be approximately 100k $\Omega$ . When

the switch pulls in, the switch becomes parallel to the circuit and brings a switch resistance that is parallel to the circuit. If we want to ignore the current on the switch, we should take the switch resistance higher than equivalent resistance of the circuit which is assumed to be approximately  $100\text{k}\Omega$ .

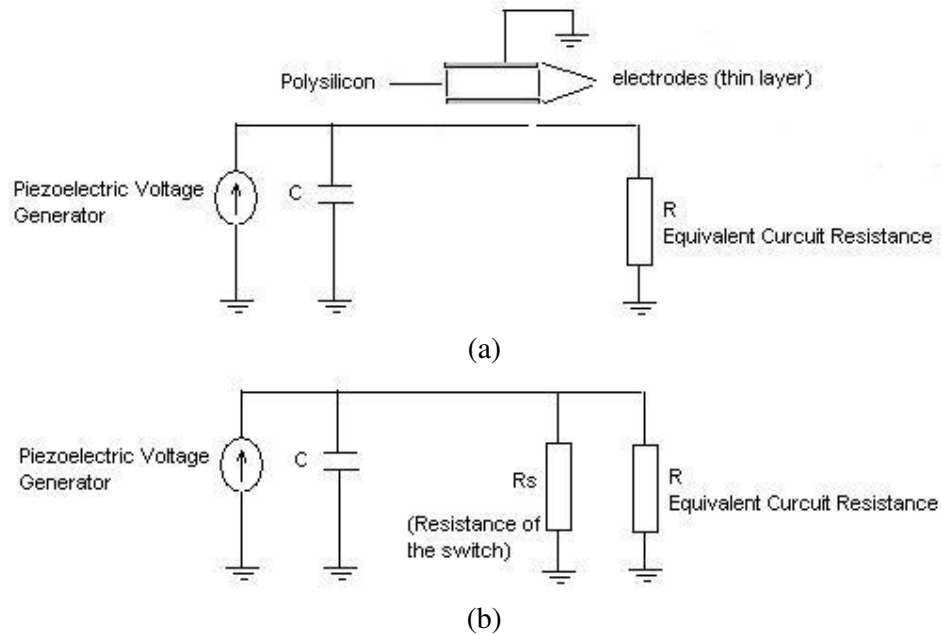


**Figure 3.47:** (a) The System While Switch is Off (b) The System While the Switch is On Position

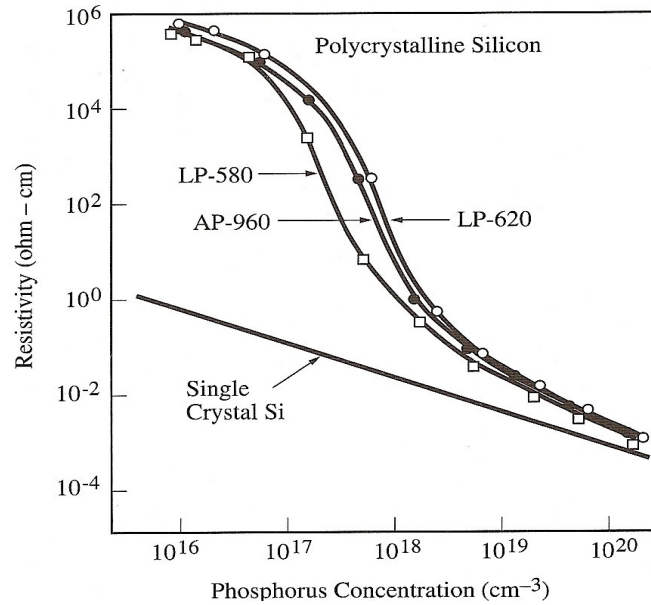


**Figure 3.48:** The Resistivity Change of Polysilicon Related to Phosphorus Concentration [23]

Resistivity of polysilicon can be decreased by doping with phosphorus. The resistivity change of Polysilicon by phosphorus concentration can be seen in Figure 3.48 where AP refers to APCVD (Atmospheric Pressure Chemical Vapor Deposition) and LP refers to LPCVD (Low Pressure Chemical Vapor Deposition) [23]. The concept for the most suitable cantilever beam can be seen in Figure 3.49. We have taken the length of the electrode below the beam as  $50\mu\text{m}$ . Taking phosphorus concentration approximately  $5 \times 10^{16} \text{cm}^{-3}$  where the resistivity of polysilicon takes its value around  $25 \times 10^3 \Omega \cdot \text{m}$ . Calculated resistance values of cantilever beams that we are concerned can be seen in Table 3.11. These values should be taken into consideration while designing power harvester system. Considering the requirements for our system, results in the table shows that using Polysilicon to fabricate the MEMS switch is convenient to obtain a switch whose resistance is relatively high and the current on it that is approximately  $0.1\mu\text{A}$  can be negligible after comparing with the current that the current on the circuit.

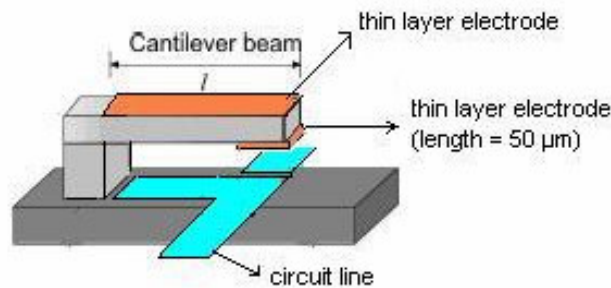


**Figure 3.49:** The Concept for the Most Suitable Cantilever Beam

**Table 3.11:** Resistance Values of Cantilever Beams

Cantilever Beam	Resistivity of Used Material ( $\Omega \cdot \text{m}$ )	Resistance ( $\Omega$ )
<b>Polysilicon Cantilever Beam</b> (Phosphorus Concentration $5 \times 10^{16} \text{cm}^{-3}$ )	$\sim 25 \times 10^3$	$10 \times 10^6$
<b>Aluminum Cantilever Beam</b>	$2.82 \times 10^{-8}$	$11.2 \times 10^{-6}$
<b>Gold Cantilever Beam</b>	$2.44 \times 10^{-8}$	$9.7 \times 10^{-6}$

#### 4. CONCLUSION AND FUTURE WORK

The main goal of this work is to design a novel MEMS switch for a power harvesting system whose core is a MEMS device with a  $100\mu\text{m}$  wide,  $5\mu\text{m}$  thick and  $3\text{mm}$  long tethers sharing a  $2.5\text{mm}$  wide,  $2.5\text{mm}$  long, and  $500\mu\text{m}$  thick proof-mass, generating approximately  $0.6\text{-}1\text{V}$  when it vibrates. Some conclusions with respect to the design and simulation of a MEMS switch can be drawn from the presented work.

Using closed form model of pull-in voltage, we simulated pull-in dynamics and optimize the size of the switch to make it suitable for voltage range of power harvester. Observing simulation results, we saw that a fixed-fixed beam is not applicable for our system because it needs higher pull-in voltage, approximately  $2.5\text{V}$ . Also, simulation results shows that the most suitable size for a cantilever beam made of Polysilicon is  $l=260\mu\text{m}$ ,  $w=50\mu\text{m}$ ,  $h=1\mu\text{m}$ ,  $d_0=1\mu\text{m}$ . Analysis for different sizes demonstrates that increase or decrease in the width value can not change pull-in voltage while other size values are constant, the optimum initial gap value is  $d_0=1\mu\text{m}$ , and optimum thickness value  $h=1\mu\text{m}$ . Moreover, analysis for different materials brings that under the same design values making the beam from aluminum brings great advantage regarding to the pull-in voltage.

We presented analytical expressions for the natural frequencies and effective masses of a cantilever beam and a fixed-fixed beam. Simulations show that resonant frequencies of cantilever beam and fixed-fixed beam are in the KHz values that are so convenient for operating conditions of the system which are in the range of  $100\text{-}200\text{Hz}$  values. Also, related to the simulation results, producing cantilever beam from Polysilicon is the most preferable. However, there is no more difference between resonant frequencies of Aluminum cantilever beam and Polysilicon cantilever beam.

To see if the cantilever beam is robust or not, we observed the responses of the cantilever beam under vibrations. This observation contains vibration analysis at zero voltage and at voltage is less than pull-in voltage. Simulations for Polysilicon,

Aluminum, and Gold cantilever beams are approximately same. It can be said that it does not make so difference to produce the cantilever beam from Polysilicon, Aluminum or Gold with respect to the tip deflection results and the pull-in voltage results for different materials under a vibration. However, the minimum percentage change of pull-in voltage is for a cantilever beam made of Polysilicon and the maximum is for a cantilever beam made of Aluminum. Thus, it may be advantageous to produce the cantilever beam from Polysilicon.

To decide whether the beam is robust under different accelerations, or not, and obtain the critical damping constant, we checked the step responses of the beam for different values of acceleration. Simulations results indicate that producing the cantilever beam from Polysilicon or aluminum is so advantageous not only for critical damping value but also for maximum deflection at these accelerations. Furthermore, simulations states that using Polysilicon makes the cantilever beam so convenient for crash conditions which high accelerations occur.

Considering that the power harvesting device will be used in vibration environments and this system needs a switch whose resistance is in high values, above results indicate that fabricating the cantilever beam from Polysilicon whose  $l=260\mu\text{m}$ ,  $w=50\mu\text{m}$ ,  $h=1\mu\text{m}$ ,  $d_0=1\mu\text{m}$  is the most preferable choice as it is so robust and the most suitable for vibration conditions and voltage range of power harvesting device. Also, its resistance is around  $10\text{M}\Omega$  showing that the current on it can be neglected after comparing with the current that the current on the circuit. Moreover, to get a hysteresis cycle the contact resistance of the cantilever beam should be small. Knowing that the pull-in voltage of the Polysilicon cantilever beam is approximately  $0.98\text{V}$ , our estimation for pull-out voltage is  $V_{\text{pull-out}} \geq 0.7\text{V}$ .

The future work includes the fabrication of the cantilever beam and its reliability studies. To fabricate the cantilever beam from Polysilicon, we should use surface micromachining process as illustrated in Appendix E. Fabricated cantilever beam should be tested in vibration environments and under accelerations in real conditions.

## REFERENCES

- [1] **Elwespoek, M. and Wiegerink R.**, 2001. *Mechanical Microsensors*, Springer, Berlin.
- [2] **Senturia, S. D.**, 2001. *Microsystem Design*, second ed., Kluwer Academic Publishers, Massachusetts.
- [3] **Kaya, T.**, 2005. A Novel Micro Piezoelectric Energy Harvesting System, *Ph.D. Thesis Progress Report-2*, Institute of Science and Technology, İstanbul Technical University, İstanbul.
- [4] **Varadan, V. M., Vinoy, K. J. and Jose, K. A.**, 2003. *RF MEMS And Their Applications*, Wiley, New York.
- [5] **Chowdhury, S., Ahmadi, M. and Miller, W.C.**, 2005. Pull-in Voltage Calculations for MEMS Sensors with Cantilevered Beams, *IEEE-NEWCAS the 3rd International Conference*, Québec City, Canada, 19-22 June, pp.143 – 146.
- [6] **Gabriel, K.J.**, 1998. Microelectromechanical systems (MEMS) tutorial, *International Test Conference*, Washington, USA, 18-23 October, pp.432 – 441.
- [7] **Akı, T.**, 2003. Micro-Electromechanical Systems, Lecture Presentation, Electrical and Electronics Engineering Department, Middle East Technical University, Ankara.
- [8] **Erdener, Ö.**, 2005. MEMS Accelerometer Design, *M.S. Thesis*, Institute of Science and Technology, İstanbul Technical University, İstanbul.
- [9] **Andreou, H.**, 2003. Handout: Introduction to MEMS, John Hopkins University, Maryland, U.S.A
- [10] **Bao, M.**, 2005. *Analysis and Design Principles of MEMS Devices*, Elsevier Ltd., Amsterdam.
- [11] **Neul, R.**, 2002. Modeling and Simulation for MEMS Design, Industrial Requirements, *Technical Proceedings of the 2002 International Conference on Modeling and Simulation of Microsystems*, Puerto Rico, USA, 22-25 April, vol.1, pp. 6-9.
- [12] **Zerazadeh, G., Tahmasebi, A. and Zubstov, M.**, 2006. Application of piezoelectric layers in electrostatic MEM actuators: controlling of pull-in voltage, *Microsystem Technologies*, 12, 1163-1170
- [13] **Kaya, T. , Koser, H. and Culurciello**, 2006. A low-voltage temperature sensor for micro-power harvesters in silicon-on-sapphire CMOS, *Electronics Letters*, vol.42, no.9.
- [14] **Kaajakari, V.**, 2004. Nonlinearity in Micromechanical Resonators: A Tutorial, <http://www.kaajakari.net>.

- [15] **Whitney, S.**, 1999. Vibrations of Cantilever Beams: Deflection, Frequency, and Research Uses, University of Nebraska-Lincoln, Nebraska.
- [16] **Chen, S., Wang, G. and Chien, M.**, 2006. Analytical modeling of piezoelectric vibration-induced micro power generator, *Mechatronics*, vol.16, issue 7, 379-387.
- [17] **Wright, P., Rabaey, J., Culler, D., Leland, E., Lai, E., Mellers, S., Montero, M., Baker, J., Otis, B., Scewczyk, R. and Roundy, S.**, Industrial and Social Applications of Wireless Sensor Nets with "Energy Scavenging" With a case study on "battery-less" tiny-temperature nodes for "smart building applications", Berkeley Wireless Research Center, Presentation Notes, California.
- [18] **Legrand, B. and Collard, D.**, 2002. Electrostatic Actuation Electromechanical Resonators, CNRS-IEMN Lille, Silicon MEMS Group, Presentation Notes, France.
- [19] **Drake, J., Jernan, H., Lutze, B. and Stuber, M.**, 1995. An Electrostatically Actuated Micro-relay, *The 8th International Conference on Solid-State Sensors and Actuators*, Stockholm, Sweden, 25-29 June, vol.2, pp. 380-383.
- [20] **Grétilat, M-A, Grétilat, F. and De Rooij, N. F.**, 1999. Micromechanical relay with electrostatic actuation and metallic contacts, *Journal of Micromechanics and Microengineering*, vol.9, issue 4, 324-331.
- [21] **Rocha, L. A., Cretu, E. and Wolffenbuttel, R. F.**, 2004. Analysis and Analytical Modeling of Static Pull-In With Application to MEMS-Based Voltage Reference and Process Monitoring, *Journal of Microelectromechanical Systems*, vol.13, issue 2, 342-354.
- [22] **Majumder, S., McGruer, N.E., Adams, G.G., Zavracky, A., Zavracky, P.M., Morrison, R.H. and Krim, J.**, 1998. Study of contacts in an electrostatically actuated microswitch, *Proceedings of the Forty-fourth IEEE Holm Conference on Electrical Contacts*, Washington, DC., USA, 26-28 October, pp.127-132.
- [23] **Plummer, J.D., Deal, M.D. and Griffies, P.B.**, 2000. Silicon VLSI Technology Fundamentals, Practice and Modeling, Printice Hall

## APPENDIX A

```
%%M-File of Pull-in voltage calculations, the optimization of the %%  
%%sizes of cantilever beam, and resonant frequency calculations %%
```

```
clear;  
clc;  
  
%%material properties%%  
eps=8.85e-12;  
E=131e9; %% young modulus  
v=0.27; %% poission's ratio  
dens =2330 ; %% density  
  
w=20e-6:1e-6:50e-6; %% width  
l=200e-6:10e-6:500e-6; %% length  
w_size=size(w);  
l_size=size(l);  
  
h=input('please give the thickness value\n');  
d0=input('please give the initial gap value\n');  
h(1:w_size(2),1)=h;  
d0(1:w_size(2),1)=d0;  
  
for i=1:w_size(2)  
    for j=1:l_size(2)  
        w_plot(i)=w(i);  
        if w(i) >= 5*h(i)  
            E_eff(i)=E/(1-v^2);  
        else  
            E_eff(i)=E;  
        end  
        bracket(i,j)=5/6/d0(i)^2+0.19/d0(i)^1.25/w(i)^0.75+0.19/d0(i)^  
            1.25/l(j)^0.75+0.4*h(i)^0.5/d0(i)^1.5/w(i);  
  
        VPI(i,j)=sqrt(2*E_eff(i)*h(i)^3*d0(i)/(8.37*eps*l(j)^4*bracket  
            (i)));  
  
        I(i,j) = (w(i)*h(i)^3)/12; %% area moment of inertia  
            of the cross section  
        m(i,j) = dens*w(i)*l(j)*h(i); %% mass  
  
        freq_cant(i,j)= (1/(2*pi))*(3.5156  
            *sqrt(E_eff(i)*I(i)/((m(i)/l(j))*l(j)^4)));  
        freq_fixed(i,j)=(1/(2*pi))*(22.373*sqrt(E_eff(i)*I(i)/(m(i)/l  
            (j))*l(j)^4));  
        meff_cant(i,j)= 0.2427*m(i);  
        meff_fixed(i,j)=0.0959*m(i);  
  
    end  
end
```

```

mesh(w,l,VPI)
xlabel('Width')
ylabel('Length')
zlabel('Pull-in Voltage')

mesh(w,l,freq_cant)
title('resonant frequency change of cantilever beam for different
values of length (l) and width (w)')
xlabel('Width')
ylabel('Length')
zlabel('Frequency')

figure,mesh(w,l,freq_fixed)
title('resonant frequency change of fixed-fixed beam for different
values of length (l) and width (w)')
xlabel('Width')
ylabel('Length')
zlabel('Frequency')

figure,mesh(w,l,meff_cant)
title('Effective mass of cantilever beam for different values of
length (l) and width (w)')
xlabel('Width')
ylabel('Length')
zlabel('effective mass')

figure,mesh(w,l,meff_fixed)
title('Effective mass of fixed-fixed beam for different values of
length (l) and width (w)')
xlabel('Width')
ylabel('Length')
zlabel('effective mass')

%% Finding optimum sizes %%
fopt = abs(VPI-1);

x=min(min(fopt));
[r,c]=find(fopt==x);
rc = [r c];

wopt=w(rc(1,1));
sprintf('The optimum value of width : %d',wopt)
lopt=l(rc(1,2));
sprintf('The optimum value of length : %d',lopt)
VPIopt=VPI(rc(1,1),rc(1,2));
sprintf('The optimum value of Pull-in Voltage : %d',VPIopt)

h=h(1,1);
d0=d0(1,1);

    if wopt >= 5*h
        E_eff=E/(1-v^2);
    else
        E_eff=E;
    end

%Pull-in voltage calculation referenced to the Comsol %
B=E_eff*h^3*d0^3;
Vpi=sqrt((4*0.07*B)/(eps*lopt^4*(1+0.42*d0/wopt)));

```

```

sprintf('The optimum value of Pull-in Voltage related to the COMSOL
: %d',Vpi)

k = (E_eff*wopt*h^3)/(4*lopt^3);           %% spring constant
b = 0.01;                                 %% damping factor
m = dens*wopt*lopt*h;                     %% mass
I = (wopt*h^3)/12;                         %%area moment of
inertia of the cross section

%% Resonant frequency calculations %%%%%%%%%%
freq_cant= (1/(2*pi))*(3.5156 *sqrt(E_eff*I/((m/lopt)*lopt^4)));
sprintf('The resonant frequency for cantilever beam : %d',freq_cant)
freq_fixed= (1/(2*pi))*(22.373*sqrt(E_eff*I/((m/lopt)*lopt^4)));
sprintf('The resonant frequency for fixed-fixed beam :
%d',freq_fixed)

```

## APPENDIX B

Consider a cantilever beam with mass per length  $\rho$ . Assume that the beam has a uniform cross section. Let's determine the natural frequency and find the effective mass, where the distributed mass is represented by a discrete, end-mass.

The governing differential equation is

$$-EI \frac{\partial^4 y}{\partial x^4} = \rho \frac{\partial^2 y}{\partial t^2} \quad (\text{B.1})$$

Separate the dependent variable.

$$y(x, t) = Y(x)T(t) \quad (\text{B.2})$$

$$-EI \frac{\partial^4 [Y(x)T(t)]}{\partial x^4} = \rho \frac{\partial^2 [Y(x)T(t)]}{\partial t^2} \quad (\text{B.3})$$

$$-EIT(t) \left\{ \frac{d^4}{dx^4} Y(x) \right\} = \rho Y(x) \left\{ \frac{d^2}{dt^2} T(t) \right\} \quad (\text{B.4})$$

$$\left\{ \frac{-EI}{\rho} \right\} \frac{\left\{ \frac{d^4}{dx^4} Y(x) \right\}}{Y(x)} = \frac{\left\{ \frac{d^2}{dt^2} T(t) \right\}}{T(t)} \quad (\text{B.5})$$

Let "c" be a constant.

$$\left\{ \frac{-EI}{\rho} \right\} \frac{\left\{ \frac{d^4}{dx^4} Y(x) \right\}}{Y(x)} = \frac{\left\{ \frac{d^2}{dt^2} T(t) \right\}}{T(t)} = -c^2 \quad (\text{B.6})$$

Separate the time variable.

$$\frac{\left\{ \frac{d^2}{dt^2} T(t) \right\}}{T(t)} = -c^2 \quad (\text{B.7})$$

$$\frac{d^2}{dt^2} T(t) + c^2 T(t) = 0 \quad (\text{B.8})$$

Separate the spatial variable.

$$\left\{ \frac{-EI}{\rho} \right\} \frac{\left\{ \frac{d^4}{dx^4} Y(x) \right\}}{Y(x)} = -c^2 \quad (\text{B.9})$$

$$\frac{d^4}{dx^4} Y(x) - c^2 \left\{ \frac{\rho}{EI} \right\} Y(x) = 0 \quad (\text{B.10})$$

A solution for Eq. (B.10) is

$$Y(x) = a_1 \sinh(\beta x) + a_2 \cosh(\beta x) + a_3 \sin(\beta x) + a_4 \cos(\beta x) \quad (\text{B.11})$$

$$\frac{dY(x)}{dx} = a_1 \beta \cosh(\beta x) + a_2 \beta \sinh(\beta x) + a_3 \beta \cos(\beta x) - a_4 \beta \sin(\beta x) \quad (\text{B.12})$$

$$\frac{d^2 Y(x)}{dx^2} = a_1 \beta^2 \sinh(\beta x) + a_2 \beta^2 \cosh(\beta x) - a_3 \beta^2 \sin(\beta x) - a_4 \beta^2 \cos(\beta x) \quad (\text{B.13})$$

$$\frac{d^3 Y(x)}{dx^3} = a_1 \beta^3 \cosh(\beta x) + a_2 \beta^3 \sinh(\beta x) - a_3 \beta^3 \cos(\beta x) + a_4 \beta^3 \sin(\beta x) \quad (\text{B.14})$$

$$\frac{d^4 Y(x)}{dx^4} = a_1 \beta^4 \sinh(\beta x) + a_2 \beta^4 \cosh(\beta x) + a_3 \beta^4 \sin(\beta x) + a_4 \beta^4 \cos(\beta x) \quad (\text{B.15})$$

Substitute Eq. (B.15) and Eq. (B.11) into Eq. (B.10).

$$\left\{ a_1 \beta^4 \sinh(\beta x) + a_2 \beta^4 \cosh(\beta x) + a_3 \beta^4 \sin(\beta x) + a_4 \beta^4 \cos(\beta x) \right\} - c^2 \left\{ \frac{\rho}{EI} \right\} \left\{ a_1 \sinh(\beta x) + a_2 \cosh(\beta x) + a_3 \sin(\beta x) + a_4 \cos(\beta x) \right\} = 0 \quad (\text{B.16})$$

$$\beta^4 \left\{ a_1 \sinh(\beta x) + a_2 \cosh(\beta x) + a_3 \sin(\beta x) + a_4 \cos(\beta x) \right\} - c^2 \left\{ \frac{\rho}{EI} \right\} \left\{ a_1 \sinh(\beta x) + a_2 \cosh(\beta x) + a_3 \sin(\beta x) + a_4 \cos(\beta x) \right\} = 0 \quad (\text{B.17})$$

The equation is satisfied if

$$\beta^4 = c^2 \left\{ \frac{\rho}{EI} \right\} \quad (\text{B.18})$$

$$\beta = \left\{ c^2 \left\{ \frac{\rho}{EI} \right\} \right\}^{\frac{1}{4}} \quad (\text{B.19})$$

The boundary conditions at the fixed end  $x=0$  are

$$y(0) = 0 \quad (\text{zero displacement}) \quad (\text{B.20})$$

$$\left. \frac{dy}{dx} \right|_{x=0} = 0 \quad (\text{zero slope}) \quad (\text{B.21})$$

The boundary conditions at the free end  $x=L$  are

$$\left. \frac{d^2 y}{dx^2} \right|_{x=L} = 0 \quad (\text{zero bending moment}) \quad (\text{B.22})$$

$$\left. \frac{d^3 y}{dx^3} \right|_{x=L} = 0 \quad (\text{zero shear force}) \quad (\text{B.23})$$

Apply Eq. (B.20) to Eq. (B.11)

$$a_2 + a_4 = 0 \quad (\text{B.24})$$

$$a_4 = -a_2 \quad (\text{B.25})$$

Apply Eq. (B.21) to Eq. (B.12)

$$a_1 + a_3 = 0 \quad (\text{B.26})$$

$$a_3 = -a_1 \quad (\text{B.27})$$

Apply Eq. (B.22) to Eq. (B.13)

$$a_1 \sinh(\beta L) + a_2 \cosh(\beta L) - a_3 \sin(\beta L) - a_4 \cos(\beta L) = 0 \quad (\text{B.28})$$

Apply Eq. (B.23) to Eq. (B.14)

$$a_1 \cosh(\beta L) + a_2 \sinh(\beta L) - a_3 \cos(\beta L) + a_4 \sin(\beta L) = 0 \quad (\text{B.29})$$

Apply Eq. (B.25) and Eq. (B.27) to Eq. (B.28)

$$a_1 \sinh(\beta L) + a_2 \cosh(\beta L) + a_1 \sin(\beta L) + a_2 \cos(\beta L) = 0 \quad (\text{B.30})$$

$$a_1 \{\sinh(\beta L) + \sin(\beta L)\} + a_2 \{\cosh(\beta L) + \cos(\beta L)\} = 0 \quad (\text{B.31})$$

Apply Eq. (B.25) and Eq. (B.27) to Eq. (B.29)

$$a_1 \cosh(\beta L) + a_2 \sinh(\beta L) + a_1 \cos(\beta L) - a_2 \sin(\beta L) = 0 \quad (\text{B.32})$$

$$a_1 \{\cosh(\beta L) + \cos(\beta L)\} + a_2 \{-\sin(\beta L) + \sinh(\beta L)\} = 0 \quad (\text{B.33})$$

Form Eq. (B.31) and Eq. (B.33) into a matrix format

$$\begin{bmatrix} \sinh(\beta L) + \sin(\beta L) & \cosh(\beta L) + \cos(\beta L) \\ \cosh(\beta L) + \cos(\beta L) & -\sin(\beta L) + \sinh(\beta L) \end{bmatrix} \begin{bmatrix} a_1 \\ a_2 \end{bmatrix} = \begin{bmatrix} 0 \\ 0 \end{bmatrix} \quad (\text{B.34})$$

By inspection, Eq. (B.34) can only be satisfied if  $a_1 = 0$  and  $a_2 = 0$ . Set the determinant to zero in order to obtain a nontrivial solution.

$$\{-\sin^2(\beta L) + \sinh^2(\beta L)\} - \{\cosh(\beta L) + \cos(\beta L)\}^2 = 0 \quad (\text{B.35})$$

$$\{-\sin^2(\beta L) + \sinh^2(\beta L)\} - \{\cos^2(\beta L) + 2\cos(\beta L)\cosh(\beta L) + \cosh^2(\beta L)\} = 0 \quad (\text{B.36})$$

$$-\sin^2(\beta L) + \sinh^2(\beta L) - \cos^2(\beta L) - 2\cos(\beta L)\cosh(\beta L) - \cosh^2(\beta L) = 0 \quad (\text{B.37})$$

$$-2 - 2\cos(\beta L)\cosh(\beta L) = 0 \quad (\text{B.38})$$

$$1 + \cos(\beta L)\cosh(\beta L) = 0 \quad (\text{B.39})$$

$$\cos(\beta L)\cosh(\beta L) = -1 \quad (\text{B.40})$$

There are multiple roots that satisfy Eq. (B.40). Thus, a subscript should be added as shown in Eq. (B.41).

$$\cos(\beta_n L)\cosh(\beta_n L) = -1 \quad (\text{B.41})$$

The subscript is an integer index. The root can be determined through a combination of graphing and numerical methods. The Newton-Rhapson is an example of an appropriate numerical method. The roots of Eq. (B.41) are summarized in Table-B.1.

**Table B.1:** The Roots of Eq. (B.41)

Roots	
Index	$\beta_n L$
n=1	1.87510
n=2	4.69409
n≥3	$(2n-1)\pi/2$

Note: the root value for  $n \geq 3$  is approximate.

Rearrange Eq. (B.19) as follows

$$c^2 = \beta_n^4 \left[ \frac{EI}{\rho} \right] \quad (\text{B.42})$$

Substitute Eq. (B.42) to Eq. (B.8)

$$\frac{d^2}{dt^2} T(t) + \left[ \beta_n^4 \left( \frac{EI}{\rho} \right) \right] T(t) = 0 \quad (\text{B.43})$$

Eq. (B.43) is satisfied by

$$T(t) = b_1 \sin \left[ \left( \beta_n^2 \left[ \frac{EI}{\rho} \right] \right) t \right] + b_2 \cos \left[ \left( \beta_n^2 \left[ \frac{EI}{\rho} \right] \right) t \right] \quad (\text{B.44})$$

The natural frequency term  $w_n$  is thus

$$w_n = \beta_n^2 \sqrt{\frac{EI}{\rho}} \quad (\text{B.45})$$

Substitute the value for the fundamental frequency from Table B.1.

$$w_1 = \left[ \frac{1.87510}{L} \right]^2 \sqrt{\frac{EI}{\rho}} = \left[ \frac{3.5156}{L^2} \right] \sqrt{\frac{EI}{\rho}} \quad (\text{B.46})$$

$$f_1 = \frac{1}{2\pi} \left[ \frac{3.5156}{L^2} \right] \sqrt{\frac{EI}{\rho}} \quad (\text{B.47})$$

The effective mass  $m_{\text{eff}}$  at the end of the beam is thus

$$m_{\text{eff}} = \frac{k}{[2\pi f_n]^2} \quad (\text{B.48})$$

$$m_{\text{eff}} = \frac{3EI}{L^3 \left[ 2\pi \left[ \frac{1}{2\pi} \left[ \frac{3.5156}{L^2} \right] \sqrt{\frac{EI}{\rho}} \right] \right]^2} \quad (\text{B.49})$$

$$m_{\text{eff}} = 0.2427 \rho L \quad (\text{B.50})$$

## APPENDIX C

Consider a fixed-fixed beam with a uniform mass density and a uniform cross section. The governing differential equation is

$$-EI \frac{\partial^4 y}{\partial x^4} = \rho \frac{\partial^2 y}{\partial t^2} \quad (\text{C.1})$$

The spatial equation is

$$\frac{d^4}{dx^4} Y(x) - c^2 \left\{ \frac{\rho}{EI} \right\} Y(x) = 0 \quad (\text{C.2})$$

The boundary conditions for fixed-fixed beam are

$$Y(0) = 0 \quad (\text{C.3})$$

$$\left. \frac{dY(x)}{dx} \right|_{x=0} = 0 \quad (\text{C.4})$$

$$Y(L) = 0 \quad (\text{C.5})$$

$$\left. \frac{dY(x)}{dx} \right|_{x=L} = 0 \quad (\text{C.6})$$

Eigenvector has the form

$$Y(x) = a_1 \sinh(\beta x) + a_2 \cosh(\beta x) + a_3 \sin(\beta x) + a_4 \cos(\beta x) \quad (\text{C.7})$$

$$\frac{dY(x)}{dx} = a_1 \beta \cosh(\beta x) + a_2 \beta \sinh(\beta x) + a_3 \beta \cos(\beta x) - a_4 \beta \sin(\beta x) \quad (\text{C.8})$$

$$\frac{d^2 Y(x)}{dx^2} = a_1 \beta^2 \sinh(\beta x) + a_2 \beta^2 \cosh(\beta x) - a_3 \beta^2 \sin(\beta x) - a_4 \beta^2 \cos(\beta x) \quad (\text{C.9})$$

$$Y(0) = 0 \quad (\text{C.10})$$

$$a_2 + a_4 = 0 \quad (\text{C.11})$$

$$a_2 = -a_4 \quad (\text{C.12})$$

$$\left. \frac{dY(x)}{dx} \right|_{x=0} = 0 \quad (\text{C.13})$$

$$a_1 * \beta + a_3 * \beta = 0 \quad (\text{C.14})$$

$$a_1 + a_3 = 0 \quad (\text{C.15})$$

$$a_1 = -a_3 \quad (\text{C.16})$$

$$Y(x) = a_1 \{ \sinh(\beta x) - \sin(\beta x) \} + a_2 \{ \cosh(\beta x) - \cos(\beta x) \} \quad (\text{C.17})$$

$$\frac{dY(x)}{dx} = a_1 * \beta \{ \cosh(\beta x) - \cos(\beta x) \} + a_2 * \beta \{ \sinh(\beta x) + \sin(\beta x) \} \quad (\text{C.18})$$

$$Y(L) = 0 \quad (\text{C.19})$$

$$a_1 \{ \sinh(\beta L) - \sin(\beta L) \} + a_2 \{ \cosh(\beta L) - \cos(\beta L) \} = 0 \quad (\text{C.20})$$

$$\left. \frac{dY(x)}{dx} \right|_{x=L} = 0 \quad (\text{C.21})$$

$$a_1 * \beta \{ \cosh(\beta L) - \cos(\beta L) \} + a_2 * \beta \{ \sinh(\beta L) + \sin(\beta L) \} = 0 \quad (\text{C.22})$$

Form Eq. (C.20) and Eq. (C.22) into a matrix format

$$\begin{bmatrix} \sinh(\beta L) - \sin(\beta L) & \cosh(\beta L) - \cos(\beta L) \\ \cosh(\beta L) - \cos(\beta L) & \sinh(\beta L) + \sin(\beta L) \end{bmatrix} \begin{bmatrix} a_1 \\ a_2 \end{bmatrix} = \begin{bmatrix} 0 \\ 0 \end{bmatrix} \quad (\text{C.23})$$

Set the determinant to zero in order to obtain a nontrivial solution.

$$\{ \sinh(\beta L) - \sin(\beta L) \} * \{ \sinh(\beta L) + \sin(\beta L) \} - \{ \cosh(\beta L) - \cos(\beta L) \}^2 = 0 \quad (\text{C.24})$$

$$\sinh^2(\beta L) - \sin^2(\beta L) - \cosh^2(\beta L) + 2 \cos(\beta L) \cosh(\beta L) - \cos^2(\beta L) = 0 \quad (\text{C.25})$$

$$2 \cos(\beta L) \cosh(\beta L) - 2 = 0 \quad (\text{C.26})$$

$$\cos(\beta L) \cosh(\beta L) - 1 = 0 \quad (\text{C.27})$$

The roots can be found via the Newton-Raphson Method. The first root is

$$\beta * L = 4.73004 \quad (\text{C.28})$$

$$w_n = \beta_n^2 * \sqrt{\frac{E * I}{\rho}} \quad (\text{C.29})$$

$$w_1 = \left[ \frac{4.73004}{L} \right]^2 \sqrt{\frac{EI}{\rho}} = \left[ \frac{22.373}{L^2} \right] \sqrt{\frac{EI}{\rho}} \quad (\text{C.30})$$

$$f_1 = \frac{1}{2\pi} \left[ \frac{22.373}{L^2} \right] \sqrt{\frac{EI}{\rho}} \quad (\text{C.31})$$

The stiffness at the center of the beam is

$$k = \frac{48 * E * I}{L^3} \quad (\text{C.32})$$

The effective mass  $m_{\text{eff}}$  at the center of the beam is thus

$$m_{\text{eff}} = \frac{k}{[2\pi f_n]^2} \quad (\text{C.33})$$

$$m_{\text{eff}} = \frac{48 * E * I}{L^3 \left[ 2\pi \left[ \frac{1}{2\pi} \left[ \frac{22.373}{L^2} \right] \sqrt{\frac{EI}{\rho}} \right] \right]^2} \quad (\text{C.34})$$

$$m_{\text{eff}} = 0.0959 \rho L \quad (\text{C.35})$$

## APPENDIX D

```
%%%%%%%% Function for tip deflection analysis %%%%%%%%%%

function [tip_defl_amp]=silicon_cantilever_tip_deflection(L,W,H,
input_def_amp, input_def_freq)

%%%dimensions
%L=length
%W=width
%H=thickness

%%% Material Properties
E = 131e9; %%% Young's Modulus
rho =2331; %%% density

% Calculations
I=(L/12)*W*(H^3);% Area moment of Inertia
Area=W*H; % Area
mass=rho*L*W*H; % Mass

% Damping coefficient
beta=0; %%%0.01;
alfa=0.001;

%frequency range
w = 2*pi*input_def_freq;

k=((rho.*Area.*(w.^2)-alfa.*j*w)./(E.*I+beta.*I*j.*w)).^0.25;

% introducing new variables
c=cos(k*L);
ch=cosh(k*L);
s=sin(k*L);
sh=sinh(k*L);

%Tip deflection
tip_amp=((input_def_amp.*(c+ch)./(c.*ch+1)));

%%% Function output
tip_defl_amp = abs(input_def_amp-tip_amp);

%%%%%%%% Commands that are used in command window %%%%%%%%%%
%freq = logspace(0,6,1000);
%input_def = 200*200*100e-6./freq/freq;
%defl = silicon_cantilever_tip_deflection(350e-6, 50e-6, 2e-6,
input_def, freq);
%semilogx(freq, defl);
```

## APPENDIX E

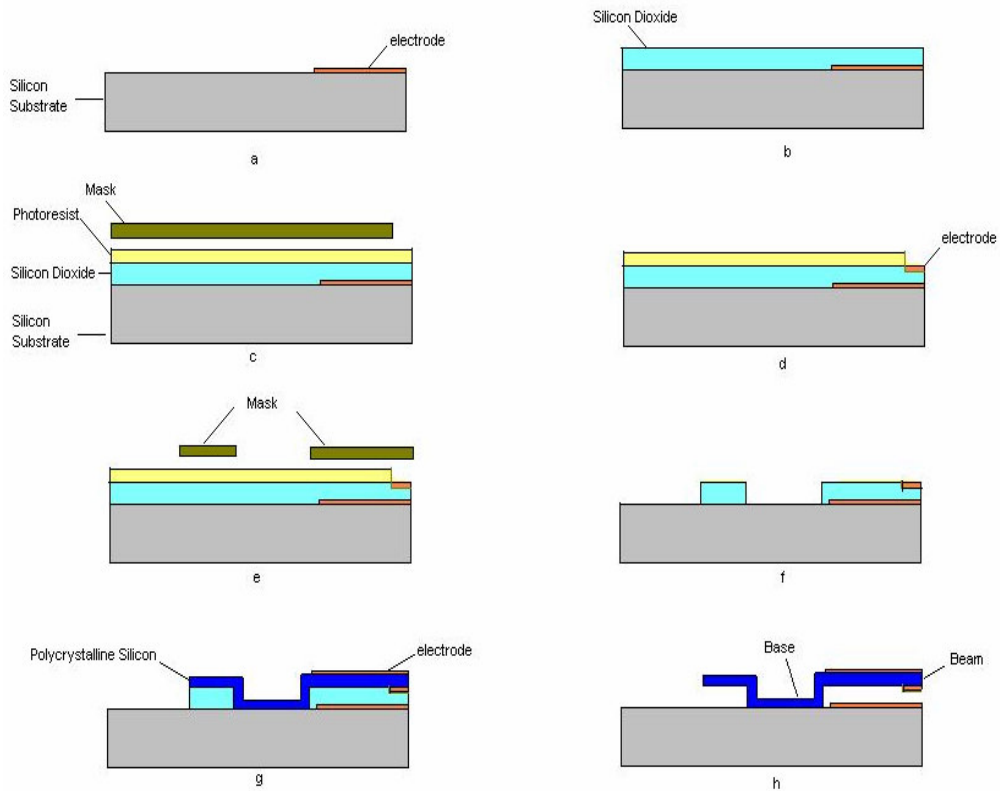


**Figure E.1:** The Fabrication Process for The Concept of The Cantilever Beam

A single cycle in common surface micro-machining process is illustrated in Figure E.1. The process to build our concept for the cantilever beam begins with putting an electrode on wafer (a). Then, the sacrificial material layer (silicon dioxide) is patterned on all over the surface (b). To make an electrode available below the beam, sacrificial material layer is etched by using photolithography (c). An electrode is put on the etched surface (d). Next, to realize the cantilever beam, the sacrificial material layer (silicon dioxide) is etched by using photolithography (e, f). After that, the structural material (polysilicon) is deposited over the entire surface and then patterned and etched in the shape of the cantilever beam and base, also an electrode is put on the beam part (g). Finally, the polysilicon is released by removing the remaining and underlying silicon dioxide (h).

## **BIOGRAPHY**

Halil TEKİN was born in 20.03.1982 in Gediz, Kütahya. He graduated from Mustafa Necip Alayeli Anatolian High School and attended Istanbul Technical University. He received B.S. degree in Control Engineering from Istanbul Technical University in 2005 with the first rank and highest honors not only in Control Engineering Program but also among all Electrical Engineering Department graduates. He gained Siemens Excellence Award and some outstanding awards for his enthusiastic and successful studies. His research interests are integrated systems like MEMS, Bio-MEMS, NEMS and application of engineering knowledge to biology. He worked as an R&D Engineer in R&D Centers of Vestel and Arçelik where he made a patent application. He is one of the few recipients of Master Degree Scholarship of Technological and Research Council of Turkey.